Binary Adsorbent Photocatalyst Hybrid Nanomaterial for Improved Degradation of Tetracycline from Water

By

Ayesha Ikram

(Registration No: 00000328449)

Department of Materials Engineering

School of Chemical and Materials Engineering

National University of Sciences & Technology (NUST)

Islamabad, Pakistan

(2024)

Binary Adsorbent Photocatalyst Hybrid Nanomaterial for Improved Degradation of Tetracycline from Water

By

Ayesha Ikram

(Registration No: 00000328449)

A thesis submitted to the National University of Sciences and Technology, Islamabad,

in partial fulfillment of the requirements for the degree of

Master of Science in
Chemical Engineering

Supervisor: Dr. Erum Pervaiz

School of Chemical and Materials Engineering

National University of Sciences & Technology (NUST)

Islamabad, Pakistan

(2024)

THESIS ACCEPTANCE CERTIFICATE

l

THESIS ACCEPTANCE CERTIFICATE

Certified that final copy of MS thesis written by Ms **Ayesha Ikram** (Registration No 00000328449), of School of Chemical & Materials Engineering (SCME) has been vetted by undersigned, found complete in all respects as per NUST Statues/Regulations, is free of plagiarism, errors, and mistakes and is accepted as partial fulfillment for award of MS degree. It is further certified that necessary amendments as pointed out by GEC members of the scholar have also been incorporated in the said thesis.

Signature: _____

Name of Supervisor: **Dr Erum Pervaiz** _____

Date: 13|3|24 _____

Signature (HOD): _____

Date: 13|3|24 _____

Signature (Dean/Principal): _____

Date: 13·3·2024 _____

TH - 1

<u>Form TH-1</u>

(Must be type written)

National University of Sciences & Technology (NUST)
MASTER'S THESIS WORK
Formulation of Guidance and Examination Committee (GEC)

Name: **AYESHA IKRAM** NUST Reg No: 00000328449

Department: **SCME** Specialization: __Chemical Engineering

Credit Hour Completed: __24__ CGPA: __3.13__

Course Work Completed

S/No	Code	Title	Core/Elective	CH	Grade
1	EME921	Momentum Heat and Mass Transport (MHMT) in Chemical Engineering	Core	3	B
2	CHE843	Separation Processes in CHE	Core	3	C+
3	CHE-848	Gasification Processes	Elective	3	B
4	RM 898	Research Methodology	Additional	2	Q
5	CHE847	Chemical Kinetics and Reactor Design	Core	3	B
6	EME981	Advanced Fuel Technology	Elective	3	B+
7	ESE-826	Industrial Catalysis for Energy Systems	Elective	3	A
8	CHE-815	Nano Catalysis	Elective	3	B
9	ESE-911	Carbon Capture and Utilization	Elective	3	B

Date: 24/02/2022 Student's Signature

Thesis Committee

1. Name: **Dr. Erum Pervaiz (Supervisor)** Signature:
   Department: **SCME**
2. Name: **Dr. Waheed Miran (Co-Supervisor)** Signature:
   Department: **SCME**
3. Name: **Dr. Sarah Farrukh (GEC)** Signature:
   Department: **SCME**
4. Name: **Dr. Sher Ahmed (GEC)** Signature:
   Department: **SCME**

Date: 29/3/22 Signature of Head of Department:

APPROVAL

Date: 29-3-no 22 Dean/Principal

Distribution
1x copy to Exam Branch, Main Office NUST
1x copy to PGP Dte, Main Office NUST
1x copy to Exam branch, respective institute

School of Chemical and Materials Engineering (SCME) Sector H-12, Islamabad

TH – 4

National University of Sciences &Technology (NUST)

MASTER'S THESIS WORK

We hereby recommend that the dissertation prepared under our supervision by

Regn No & Name: <u>00000328449 Ayesha Ikram</u>

Title: <u>Binary nanohybrid (CdS @ ZIF-67 & g-C3N4@CdS) Photocatalyst for Tetracycline removal using Advanced Oxidation Process.</u>

Presented on: <u>01 Feb 2024</u>   at: <u>1430 hrs in SCME Seminar Hall</u>

Be accepted in partial fulfillment of the requirements for the award of Master of Science degree in <u>Chemical Engineering</u>.

Guidance & Examination Committee Members

Name: **Dr Sher Ahmed**   Signature:_____

Name: **Dr Sarah Farrukh**   Signature:_____

Name: **Dr Waheed Miran** (Co-Supervisor)   Signature:_____

Supervisor's Name: <u>Dr Erum Pervaiz</u>   Signature:_____

Dated: __16/2/24__

Head of Department
Date __16/2/24__

Dean/Principal
Date __16. 2. 2024.__

School of Chemical &Materials Engineering (SCME)

AUTHOR'S DECLARATION

With this statement, I, Ayesha Ikram, declare that my master's thesis, entitled "Binary Adsorbent Photocatalyst Hybrid Nanomaterial for Improved Degradation of Tetracycline from Water" is my original work that I haven't submitted before to the National University of Sciences and Technology in Islamabad, Pakistan, or any other place in the world.

The university has the right to revoke my MS degree at any point, even after I graduate, if it turns out that my statement was false.
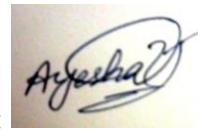
Name of Student: Ayesha Ikram

Date: 12-03-2024

PLAGIARISM UNDERTAKING

I hereby formally affirm that the research described in this thesis is "Binary Adsorbent Photocatalyst Hybrid Nanomaterial for Improved Degradation of Tetracycline from Water" is entirely my own research, with no noteworthy assistance from other individuals. I have written a complete thesis and I have duly acknowledged any minor contributions or help which I received.

I am conscious of the National University of Sciences and Technology (NUST), Islamabad, and HEC's zero-tolerance stance regarding plagiarism. As a result, I, author of thesis, with same title, hereby declare that my thesis has not been copied in any way and that all sources have been properly cited.

I agree, HEC and NUST, Islamabad have right to publish my name on HEC/University website, that lists the names of students who turned in plagiarized theses, and that University reserves right to revoke my MS degree, if I am, found guilty of formal plagiarism in mentioned thesis, even after I have received degree.

Student Signature: _____

Name: Ayesha Ikram

DEDICATION

This study is honoring my parents who have always provided me with direction and encouragement. To my supervisor who shared her knowledge, gave advice, and encouraged me to fulfill my objectives. And to all my fellows I worked with whom I've enjoyed wonderful memories.

ACKNOWLEDGEMENTS

TABLE OF CONTENTS

LIST OF TABLES

LIST OF FIGURES

LIST OF SYMBOLS, ABBREVIATIONS AND ACRONYMS

TC	Tetracycline
g-C$_3$N$_4$	Graphitic Carbon Nitride
CdS	Cadmium Sulfide
ZIF	Zeolitic Imidazolate Framework
MOF	Metal Organic Framework
GC	g-C$_3$N$_4$/CdS
CZ	CdS/ZIF-67
XRD	X-ray Diffraction
SEM	Scanning Electron Microscopy
VB	Valence Bound
CB	Conduction Bound

ABSTRACT

Water contamination is a major worldwide issue that endangers human and environmental health at risk. Water supplies are rendered unfit for intake or reuse by pollutants like as organic waste & heavy metals, necessitating efficient wastewater treatment techniques. For this issue, several solutions have been put forth, namely membrane separation, adsorption, & photocatalysis. Photocatalysis is an innovative method in which nano-adsorbent particles degrade tetracycline (TC) without the usage of any further treatment. Antibiotic usage has significantly increased recently because of bacterial infectious diseases that affect both humans and animals. But this use is resulting in harmful effects to the water quality, aquatic environment, and soil microbial communities. In this work, I have focused on the tetracycline removal from water using advanced oxidation process by synthesizing efficient nanohybrids. The most effective way to treat water so that it can be used again for irrigation and drinking is the advanced oxidation process. These nanohybrids act both as photocatalyst and adsorbent thereby enhancing the percentage degradation of tetracycline. This study created a new photo-adsorbent via a hydrothermal and in-situ technique. Results of X-ray diffraction and scanning electron microscopy show that photo-absorbents are synthesized efficiently. UV-Visible spectrophotometry is used to evaluate degradation performance. By using 100 mg of CdS@ZIF-67 hybrid, 96% of tetracycline has been successfully degraded in 110 minutes. By increasing the quantity of CdS, percentage removal of tetracycline has been increased. CdS is found to be potential highly efficient photocatalyst for tetracycline degradation.

CHAPTER 1:   INTRODUCTION

1.1 Background

The evidence that pharmaceutical antibiotics are part of a class of extremely toxic pollutants has brought increased attention to these drugs, which are widely used in medical therapy and agriculture worldwide, in recent years [1]. Given that many Merely absorbed antibiotics, such as tetracyclines, and metabolized by animals and patients they treat, a significant portion of them is expelled through feces and urine as the original parent component. In the downstream river near the 10 million city of Lahore, high concentrations of antibiotics were found to be "2700, 1700, and 1100 ng L^{-1}" for "sulfamethoxazole, trimethoprim and oxytetracycline", in that order. With measured levels of "1100, 4100, 6200, 7300, 8000, 27000, 28000, and 49000 ng L^{-1}," respectively, a facility of making drugs had the highest amounts of "erythromycin, lincomycin, ciprofloxacin, ofloxacin, levofloxacin, oxytetracycline, trimethoprim, and sulfamethoxazole" [2].Tetracycline is the second most consumed and produced antibiotic worldwide due to some exceptional properties like nontoxic nature, broad spectrum activity, and economic in nature. TC has been widely used and has a high adsorption capacity, which has led to its frequent detection in both surface and groundwater [3].

On the other hand, domestic wastewater contains antibiotic residue because wastewater treatment facilities are unable to remove these micropollutants from the wastewater [4]. This antibiotic residue may exist as a parent drug, a metabolite, Sometimes it occurs as a TC-metal complex within their environment's water matrix, and it may pose serious environmental risks to animals and humans as a kind of antibiotic-resistant bacteria or emergence of new disease [5]. Therefore, searching for immediate alternative techniques that are cost-effective and environmentally sustainable for removing TC from wastewater is essential. It is critically necessary to gain a better understanding of tetracycline residues in water matrix of environment, since they may contribute to the emergence of bacteria and genes resistant to TC [6].
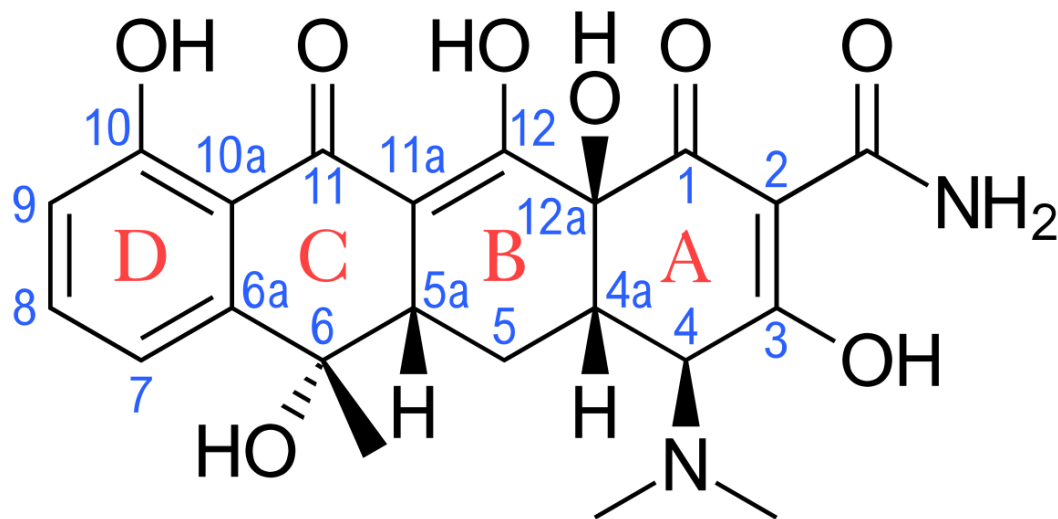
Figure 1.1: Structure of Tetracycline

Diverse methods were employed by numerous researchers to extract TC from water. For example, Photolysis, photo-Fenton, Fenton, ozonation reactions, as well as antibiotic oxidation in existence of ozone/ultraviolet/hydrogen peroxide light [7]. Among them the best technique with the greater efficiency is the technique of photocatalysis [8]. In Photocatalysis a light driven reaction is used to remove TC from the solution with the help of some catalyst. Different catalysts have been used for this like recto rite, coal humic acid, single-walled-carbon-nanotubes, chitosan particles, montmorillonite, multi-walled-carbon-nanotubes, palygorskite (hydrated magnesium aluminum silicate). But in order to remove these contaminants, there is increasing need for development of effective and affordable remediation technologies. [9].

Cadmium Sulfide (CdS) has significantly increased interest in the recent year because of low cost, and remarkable catalytic performance. The CB energy level of CdS, which is 0.41 eV is significantly, more negative than potential for hydrogen evolution, suggesting that organic pollutant photodegradation and H_2 evolution are promising prospects. [1]. CdS-based hybrids with different materials for a variety of applications have been credited with exceptional results [10]. Despite these properties photo-corrosion is the

biggest problem related to CdS. A number of techniques are being employed to address this issue, including heterojunction creation, heteroatom doping and loading of co-catalyst, as well as the introduction of various components to satisfy heterojunction creation or to differ the electron motion to enhance their properties and for their activity [11, 12]. Ag/TiO_2 nanoparticles on the exterior and microorganisms on the inside of polyurethane cubes, which were being employed as transporters allowed Xiong et al. to degrade TC using a combined photocatalysis and biodegradation system [12]. Cadmium sulfides and carbon nitride nanocomposite ($CdS/g-C_3N_4$) were synthesized by pulsed liquid ablation in liquid. CdS nanostructures are grown on graphitic carbon nitride nanosheets [13]. Graphitic carbon nitride ($g-C_3N_4$) a prominent photocatalyst for environmental remediation and semiconductor-based photocatalyst [14, 15]. The $g-C_3N_4$ demonstrated band gap 2.7eV, indicating greater visible light absorption [16]. The strong covalent connection that exists between carbon and nitrogen atoms in conjugated $g-C_3N_4$ framework, $g-C_3N_4$ possesses relatively greater thermal and chemical stability [17]. Regardless of these benefits, $g-C_3N_4$ catalytic activity is hindered by a lower reusability, a smaller surface area, and higher ratio of recombination of charge carrier [18].

$g-C_3N_4$ has gained popularity recently a non-metallic, visible light activated semiconductor and has garnered a lot of interest as a potentially useful substance for a range of environmental remediation applications [19, 20]. Of the seven phases of carbon nitride, $g-C_3N_4$ has the most stability at room temperature and has 2D layered allotrope like graphite. This allotrope has drawn a lot of interest. $g-C_3N_4$ consists of tri-s-triazine or s-triazine units, which are building blocks connected by tertiary amines, to create π-conjugation system. One can create $g-C_3N_4$ among a range of N- and C-rich precursors [21] using different methodologies [22, 23]. Numerous investigations have been carried out to examine the effects of the precursors and treatment processes on morphology, structure, and optical and physicochemical properties of $g-C_3N_4$ [24] [25].

The tertiary amino groups that link the π-conjugated layers make it easier to modify $g-C_3N_4$ to be able to boost specific surface area and electron mobility [26, 27]. This semiconductor's tunable band gap enhances its metal doping adaptability, enabling it to produce more active sites and form heterojunctions with other semiconductors, thereby

expanding its application range and photocatalytic activity [28]. Moreover, g-C$_3$N$_4$ has outstanding thermal endurance to six hundred degree Celsius, water resistivity, super-hardness, and high chemical resistance, especially in harsh media [29]. Due to these exceptional qualities, g-C$_3$N$_4$ has been thoroughly investigated in a great deal of research as the most alluring non-metallic visible light activated photocatalyst. Although g-C$_3$N$_4$ has been subject of numerous reviews, many of them focus on describing its structure, physicochemical properties, or use in straightforward photocatalysis for water treatment. A recent publication discussed the application of g-C$_3$N$_4$ to advanced oxidation processes (AOPs) to degrade of organic contaminants present in water [30, 31]. Nevertheless, uses of g-C$_3$N$_4$ have expanded beyond straightforward photocatalysis procedures for encompassing alternative H$_2$O treatment systems, like utilizing hybrid AOP-photocatalysis and photo electrocatalysis (PEC). Thus, more conversation is warranted regarding these additional crucial uses for g-C$_3$N$_4$. Because of its π-conjugated system's layered, planar structure, g-C$_3$N$_4$ is preferred as adsorbent for aromatic pollutants and heavy metals [32]. Furthermore, g-C$_3$N$_4$'s distinct electronic structure, high chemical stability, excellent material compatibility, and adaptability in morphological modification make it the perfect material for high-performance PEC electrodes and catalytic activation of oxidants [33].

However, because of its poor electrical conductivity, rapid charge carrier recombination, and inefficient absorption of solar light, bulk g-C$_3$N$_4$'s photocatalytic activity is far from satisfactory for practical applications [34]. Generally speaking, surface active sites distribution, mass transport mechanisms, catalyst morphologies, and visible light absorption capacity are primary factors influencing photocatalytic reactions [35]. Therefore, significant efforts have been made to alter g-C$_3$N$_4$ to achieve a moderate electronic energy level and exceptional surface properties. These efforts include heteroatom doping, designing nanostructures, and incorporating other materials [36, 37]. Among them, creating target-specific morphologies or heterojunctions in nanostructure materials appears to be an efficient modification technique to maximize its photoactivity. This will introduce an internal electric field or conducting media that will inhibit photoinduced charge-carrier recombination [38, 39]. Regarding the creation of nanoarchitecture design, several synthetic pathways, including supramolecular self-assembly and exfoliation strategies, have been investigated to achieve controllable

morphologies of g-C_3N_4. Therefore, to modify g-C_3N_4 and achieve better performances, it is essential to create tailoring nanostructures with surface functionality and appropriate interfacial contacts at heterojunctions [35, 40, 41].

Especially in the last few years, several noteworthy and intriguing discoveries regarding the superior architectures of g-C_3N_4 and its hybrid composites have been reported to date. Even though several outstanding reviews have been published regarding the efficient modification of pure g-C_3N_4 for the treatment of wastewater [42, 43]. It is urgently necessary to conduct a thorough and systematic review of heterojunction design and construction to spur additional advancements for its intended photocatalytic applications. This review has not yet been published. g-C_3N_4-based multicomponent systems are covered, such as heterostructures made of metal and g-C_3N_4, nanohybrids made of inorganic semiconductor and g-C_3N_4, hybrids made of g-C_3N_4 and C-based materials, multifarious complex hybrids, and so forth. Next, functional nanostructure designs for graphene-(C_3N_4) are also showcased. These include porous structures, 2D g-C_3N_4 nanosheets, 1D g-C_3N_4 nanomaterials (such as nanotubes, nanofibers, and nanowires), and other tunable morphologies. Lastly, a succinct overview of upcoming challenges and some stimulating viewpoints on further studies concerning the creation of visible-light-induced g-C_3N-based photocatalysts are presented. Recent developments in materials science and engineering research have aided in the advancement of g-C_3N_4's use in water purification [44]. A new integrated PEC system with a g-C_3N_4-based membrane photoanode demonstrated improved antifouling properties and a phenol removal capacity ten times greater than that of a standard filtration system. [45]. In this article, we give a thorough review of the most recent uses of g-C_3N_4-based materials for oxidation and photo-electrocatalysis-based water treatment systems, as well as their removal mechanisms and performances. Specifically, the functions of g-C_3N_4 in the systems of enhanced photo-electrocatalysis and oxidizing agent activation are also emphasized. This review ends with an overview of the main obstacles to and prospects for further research on the uses of g-C_3N_4-based materials in water treatment, as well as our assessment of these materials' prospects.

Recent years have seen a notable increase in interest in cadmium sulfide (CdS) due to its exceptional catalytic activity and reasonable cost. The conduction band energy level (ECB) of CdS, which is 0.41 eV, is significantly more negative than the potential for hydrogen evolution, suggesting that organic pollutant photodegradation and H_2 evolution are promising prospects [1]. Its excellent visible light response, charge transfer capabilities, and suitable energy band structure have led to its widespread application in photocatalytic water purification and H_2 evolution. CdS-based hybrids with various materials have demonstrated remarkable performance for a range of applications [46]. Despite these qualities, the largest issue with CdS is photo-corrosion. Several methods are being used to deal with this problem, such as the formation of heterojunctions, the loading of co-catalyst, the doping of heteroatoms, and the introduction of different components to ensure heterojunction formation or to change the electron motion for their activity and improve their characteristics [11] [47]. Ag/TiO_2 nanoparticles on the exterior and microorganisms on the inside of polyurethane cubes, which were used as carriers, allowed Xiong et al. to degrade TC using a combined photocatalysis and biodegradation system. The intimately coupled photocatalysis and biodegradation (ICPB) system's TC removal efficiency approached 95% when sodium acetate was employed as a co-substrate [47]. Cadmium sulfide nanostructures are grown on graphitic carbon nitride nanosheets. It has reduced electron hole pair recombination and increased visible light absorption [48].

An emerging material called "ZIF-67", a subclass of MOF, is made up of "divalent ions (Co)" connected by an organic linker. In MOF, "metal-ligand-metal bonds" resemble Si-O-Si bonds, which result in topologies resembling zeolites. More than 150 ZIFs have been created to date and are employed in a variety of applications as cutting-edge functional materials [49, 50]. It was shown that "MOF-235, MIL-53, ZIF-67, and ZIF-8" exhibited photocatalytic activity [46] [51, 52] . Of them, ZIF-67 is thought to be a photocatalyst because of its several absorption bands in the UV-VIS-near-IR region [53] [54]. ZIF-67 exhibits a photocatalytic band gap of 1.98 eV, whereas ZIF-8 has a band gap of 4 eV due to ligand to metal transfer. It has good thermal and chemical stability [55].

1.1.1   *Photocatalysis*

Photo catalyst can be described by four main steps. Four steps are as follows:

1. Effective absorption of photons of light to create hole and electrons
2. Segregation of charges which are excited
3. electron migration to photo catalyst's exterior surface
4. migration of holes on photo catalysts
5. Initiation of reduction oxidation reaction by using hole and subsequently electrons.

The third step signifies progress and survival of photocatalytic process. It basically talks about the recombined of photoexcitation. The larger the time for photoemission to exist as hole pair in separated state higher would be the efficacy of process. Most of catalyst when the rate of recombining is high the photocatalysis process decays[56].
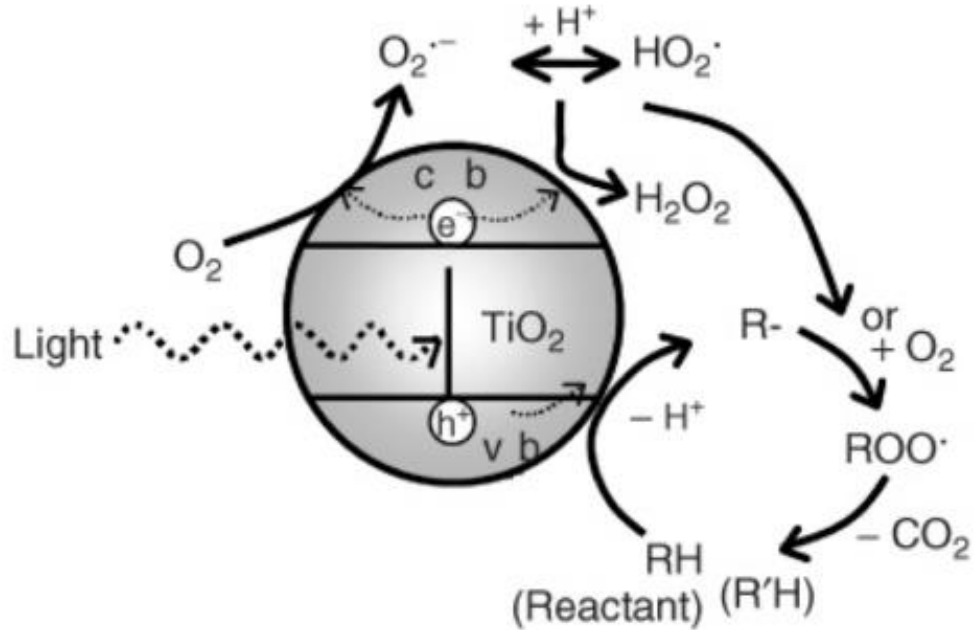
Figure 1.2: Photocatalysis reaction schematic diagram.

1.1.2   Advance Oxidation Process

Surface of photo catalyst semiconductor material contain water.it is commonly knowns absorbed water. This water which is acting as reaction medium is susceptible to oxidation by positive holes created by photoexcitation process in valence band of semiconductor. This reaction produces hydroxyl radicals, which can oxidize organic materials.

Dissolved oxygen is also present in photocatalyst reaction[57]. Electrons convert the dissolved oxygen to oxygen radicals which are necessary so that charge recombination can be avoided. Superoxide. Anions get linked or attracted to the intermediates in oxidation reaction and then form peroxide. Peroxide further transform to hydrogen peroxide[58]. The last stage in turning hydrogen peroxide into water. In organic material, the reduction is likely to happen more easily than in water. There will be more positive holes because of the higher organic matter concentration. This brings down the carrier recombination.it increases the activity of photocatalyst. This process led to complete mineralization to form carbon dioxide and water. This process is called as advance oxidation. [59]

1.2 Problem Statement

The increasing crisis of global water scarcity is having an impact on ecosystems, agriculture, and human populations across the globe. More than 2 billion people experience water scarcity because of declining freshwater resources. Numerous factors are contributing to the intensification of this crisis: pollution is poisoning available water sources, rapid urbanization is straining the supply, and climate change is changing precipitation patterns. Antibiotics play a major role in water scarcity when they are present in water sources for a variety of reasons. The widespread use of antibiotics in agriculture and livestock farming is one important factor. These antibiotics frequently contaminate surface and groundwater when they enter water systems through runoff from farms or improper disposal of animal waste. Another factor in this problem is the overuse of antibiotics in medical care. Antibiotics can enter water bodies through improper disposal of leftover medication or wastewater from pharmaceutical and medical facilities that has not been properly treated.

Conventional methods used to remove antibiotics are membrane technology, ozonation etc., but they have plenty of drawbacks. Fouling, in which the drug compounds clog or block the membrane pores, can result from the degradation of tetracycline using membranes. This lowers process efficiency and necessitates frequent membrane replacement or cleaning, which can raise operating expenses. Membrane technology has the potential to affect water quality because it can remove beneficial compounds or essential ions from the water in addition to tetracycline. Water must be forced through membranes, which can be an energy-intensive process depending on the size and kind of membrane used. This increases operating costs and the environmental impact of the process. Tetracycline molecules might not be entirely broken down by ozonation, which could result in the generation of transformation products that may remain biologically active or dangerous for the environment. Hazardous byproducts may result from ozonation, especially if the water also contains other organic materials. A few of these byproducts might be more harmful than the tetracycline compound itself. The production of ozone uses a lot of energy and specific machinery. Installing and running it can be expensive, particularly for large-scale water treatment plants. So, there is a need for a more effective method. In this research CdS based hybrids will be used as a catalyst to degrade tetracycline from wastewater as CdS is potential photocatalyst due to its photocatalytic properties. The Advanced oxidation method will be used in this research which is basically degradation of tetracycline through heterogeneous photocatalysis.

1.3 Research Objectives

The research objective is as follow:

1. Synthesis of efficient hybrid structure for removal of TC from water

2. Physical and chemical characterization techniques of the prepared hybrid structure i.e., XRD and SEM analysis

3. Kinetic study for TC removal from water

1.4 Scope of Study

Pakistan is a developing country with a scarcity of clean and pure water. The abundance of various pollutants within water sources puts a threat to both the human and environmental well-being, making the water unsuitable for consumption or any other form of reuse. To resolve this issue, this work will play an important role. 96% tetracycline has been successfully degraded from wastewater to provide clean water for drinking and irrigation purposes. One of the best advantages is that catalyst synthesized is reusable and is highly efficient even after a few times use.

1.5 Chapter Summary

This thesis consists of 5 chapters. The acquaintance of each chapter is given in the following chapters.

1. **Chapter 1** delivers a vision of subject, background and contemporary problems related to the work. It also clarifies the problem statement, research objectives and the planned study's scope.

2. **Chapter 2** will outline the results of the literature review completed to describe the previous work done on the synthesis of photocatalytic hybrids, previous method techniques and tetracycline degradation. It also includes review based to compare g-C_3N_4 based hybrids with different hybrid photocatalysts.

3. **Chapter 3** covers the methodology related to the synthesis of pure CdS, pure g-C_3N_4, pure ZIF-67 and hybrids.

4. **Chapter 4** expands on the discussion and outcome. The phases of crystal structures, and morphology of synthesized catalysts are described by analysis using XRD and SEM. The photocatalytic studies of the active catalysts and their stability also elaborated in this chapter.

5. **Chapter 5** reviews all findings and conclusions in the current study and provides the future recommendation for the related work.

CHAPTER 2: LITERATURE REVIEW

2.1 Background

Table 2.1: Different Photocatalyst and Their Removal Efficiency

g-C$_3$N$_4$ based materials	Mechanisms	Conditions	Pollutants	Removal efficiency/ Sorption capacity	Ref.
Cu$_2$MoS$_4$/ g-C$_3$N$_4$	Adsorption	Solid: 0.3 g L^{-1}	Rhodamine B (50 mg L^{-1})	420.2 mg g^{-1}	[60]
mpg-C$_3$N$_4$	Adsorption	Solid: 1 g L^{-1} pH= 4.0	Th (IV) (250 mg L^{-1})	93.53%/196.08 mg g^{-1}	[61]
CM-CN	Photocatalysis	Solid: 1 g L^{-1} Illumination: 300 W Xe lamp (400 < λ < 800 nm)	Rhodamine B (20 mg L^{-1}) Tetracycline (20 mg L^{-1})	100% in 15 min over 60% in 15 min	[62]
Eu-CN	Photocatalysis	Solid: 0.2 g L^{-1} Illumination: 300 W Xe lamp (λ ≥ 420 nm)	Tetracycline (20 mg L^{-1}) Rhodamine B (10 mg L^{-1})	82% in 50 min 98% in 50 min	[63]
K-CN	Photocatalysis	Solid: 0.4 g L^{-1} Illumination: 300 W Xe lamp (λ ≥ 420 nm)	Tetracycline (10 mg L^{-1})	83% in 90 min	[64]
CN_S	Photocatalysis	Solid: 0.2 g L^{-1} Illumination: 6 W LED lamp (λ ≥ 420 nm)	Tetracycline (20 mg L^{-1})	70% in 180 min 90% in 180 min	[65]

g-C$_3$N$_4$ based materials	Mechanisms	Conditions	Pollutants	Removal efficiency/ Sorption capacity	Ref.
			Rhodamine B (5 mg L^{-1})		

2.1.1 *g-C$_3$N$_4$-based Materials for Wastewater Remediation and Pollutants Removal*

Since g-C$_3$N$_4$-based materials have a suitable band gap, many reactive sites and high chemical stability, and are thought to be the best materials for eliminating a variety of contaminants from wastewater, organics, and heavy metal ions. Additionally, they have been extensively used in the fields of pollutant removal and water remediation.

2.1.2 *g-C$_3$N$_4$-based Materials for Removing Organic Pollutants*

Numerous hazardous and flammable contaminants, including pesticides and dyes have been discharged into environment, resulting in significant damage. Furthermore, one of main obstacles in field of environmental repair is now pollution. g-C$_3$N$_4$-based materials are primarily used in adsorption, photocatalysis, and synergistic adsorption, and photocatalysis treatment to remove organic pollutants from wastewater.

2.1.3 *Metal/g-C$_3$N$_4$- Heterostructure*

Generally speaking, it is a good idea to decorate g-C$_3$N$_4$ with noble or non-noble metal nanoparticles (NPs) to increase its photodegradation activity by increasing visible light absorption and creating a coherent interface [66]. To date, numerous researchers have altered g-C$_3$N$_4$ by adding metal nanoparticles (such as Ag, Au, Pt, Pd, and Ni) to its surface in order to remove organic contaminants from wastewater that is exposed to visible light [67, 68]. Yang and colleagues produced Ag/g-C$_3$N$_4$ by employing AgNO$_3$ and urea as precursors and silver sources, respectively, in a combined thermal polymerization and photo-deposition procedure Heterostructure formation resulted from sphere-like Ag NPs

being uniformly loaded on the g-C_3N_4 surface following exposure to a 300 W Xe lamp. Ag/g-C_3N_4 clearly showed an increase in photocurrent and an extension of the visible light response from 450 nm to 800 nm when compared to pure g-C_3N_4. This suggested that higher light absorption and quicker charge separation upon g-C_3N_4's close contact with Ag resulted in higher photodegradation efficiencies for methyl orange (MO) and p-nitrophenol (PNP). Additionally, Ag NPs could be widely distributed on g-C_3N_4 in the presence of NaBH4 as a reducing agent [69, 70]. According to Tian et al., the agglomeration of excess Ag as e-h+ recombination sites caused a noticeable decrease in the photocatalytic activities of these samples with increasing Ag NPs contents after the Ag loading amount was increased to 0.048% [70]. Ag48/C_3N_4 showed the highest photocatalytic activity at the ideal Ag loading amount (0.048%) and could completely degrade rhodamine B (RhB) under visible light irradiation in 60 minutes, whereas only 30% was removed for raw g-C_3N_4 after 180 minutes [70].

2.2 Techniques to Remove Tetracycline

2.2.1 Adsorption

Adsorbent-based wastewater treatment has emerged as one of the most successful techniques. The excellent characteristics of g-C_3N_4-based materials include their high specific surface area, an abundance of functional groups, and active sites. These interactions, which can include hydrogen bonding, hydrophobic interaction, electrostatic attraction, and others, allow the materials and pollutants to effectively remove organic pollutants from wastewater. Furthermore, the structure of organic pollutants, the solution environment, and the functional groups and structures on the surface of g-C_3N_4-based materials are all strongly correlated with the adsorption performance [71]. g-C_3N_4's multifunctional groups, defect sites, and 2D layered structure make it a superior adsorbent. Strong electrostatic attraction allowed the two-dimensional porous g-C_3N_4 nanosheets produced using an acidic hydrothermal process to perform well in selectively adsorbing anionic methyl orange [9]. Additionally, rhodamine B, methyl orange, and other organic dyes demonstrated good adsorption performance at the g-C_3N_4-ZnO@graphene aerogel heterojunction, providing a solid foundation for additional photocatalytic degradation

[72]. At a pH of 6, the g-C_3N_4/MoO_3 nanocomposites, which were created using the co-precipitation method, demonstrated an adsorption capacity of 162 mg/g^{-1} for 300 mg/L^{-1} diclofenac [73]. A one-step hydrothermal method was used to fabricate the Cu_2MoS_4/g-C_3N_4, which has a unique flower structure. This material demonstrated good cycle stability and higher adsorption properties than other adsorbents, with rhodamine B adsorption reaching 420.2 mg/g^{-1} [60]. However, because organic molecular structures are so similar, g-C_3N_4-based materials still face difficulties in the selective adsorption of organic pollutants [71].

2.2.2   *Photocatalysis*

When exposed to visible light, g-C_3N_4-based materials with an appropriate optical bandgap and strong light absorption capacity can effectively mineralize organic pollutants into non-toxic compounds like CO_2 and H_2O. Several researchers have investigated its use in water remediation. After 15 minutes of exposure to visible light, the porous g-C_3N_4 nanosheets made from the thermal condensation of melamine and cyanuric acid exhibited excellent degradation activity against tetracycline (above 60%) and rhodamine B (100%), primarily because of the superoxide radicals and holes produced by the photocatalytic process [62]. The Eu(III)-doped g-C_3N_4 has a higher carrier separation efficiency and tetracycline and rhodamine B degradation rates in wastewater as high as 82% and 98%, respectively, thanks to the synergistic effect of Eu(III) doping and hollow structure [74]. Furthermore, the Ag-deposited g-C_3N_4 shows a 3.15-fold increase in bisphenol A degradation efficiency compared to the pristine g-C_3N_4 because of the Schottky barrier formation at the interface, which facilitates the separation of photogenerated carrier [75]. The g-C_3N_4/CdS/$Bi_4O_5I_2$ heterojunction offers several pathways for photogenerated charge transfer and has the ability to break down acetaminophen at a rate of 80% in less than 25 minutes [76]. Additionally, Li et al. used the as-prepared CDs/g-C_3N_4/SnO_2 composites for the photocatalytic degradation of indomethacin under visible light irradiation, utilizing the special up-conversion photoluminescence properties and effective charge separation ability of CDs. The degradation rate was 5.62 times higher than that of pristine g-C_3N_4 [77].

2.2.3 Adsorption and Photocatalysis Synergistic Treatment

Due to their superior structural qualities, g-C_3N_4-based materials also exhibit synergistic adsorption and photocatalysis of organic pollutants in wastewater (first enriching and adsorbing organic pollutants, followed by photocatalytic decomposition and mineralization of organic pollutants). This can effectively address issues with adsorption saturation and regeneration and achieve long-term recycling. In a two-step hydrothermal process, a 3D–2D–3D BiOI/porous g-C_3N_4 /graphene hydrogel composite photocatalyst was created. It demonstrated good adsorption performance and charge separation ability, as well as straightforward recycling. The synergistic degradation efficiencies of methylene blue and levofloxacin hydrochloride when applied to a static wastewater system were 7.2 and 2.7 times higher than that of BiOI, respectively [78].

2.2.4 Membrane Technology

Membrane is selective barrier to remove the particle from incoming stream. Today membrane hybrid system is used for removing pharmaceutical. MBR is a replaced version of activated sludge technology. MBR is essentially composed of convention treatment facility mostly biological treatment coupled with physical liquid and solid separation membrane system. Membrane bioreactors combine membrane techniques like microfiltration or ultrafiltration with biological wastewater treatment methods like activated sludge. These days, a lot of wastewater treatment facilities in cities and businesses use these technologies. MBR is better as compared to activated sludge technology in following ways:

1. can manage high flow rate as compared to activated sludge.
2. has high volumetric rates
3. has high hydraulic retention times
4. has high solid retention time
5. leads to less sludge production
6. It has potential for denitrification/nitrification.

15

Most of the applications to treat wastewater by using MBR come in two types of configurations. As shown in figure the diagram of left side represents the submerged MBR system whereas the diagram of right side is known as external MBR configuration.[79-81]
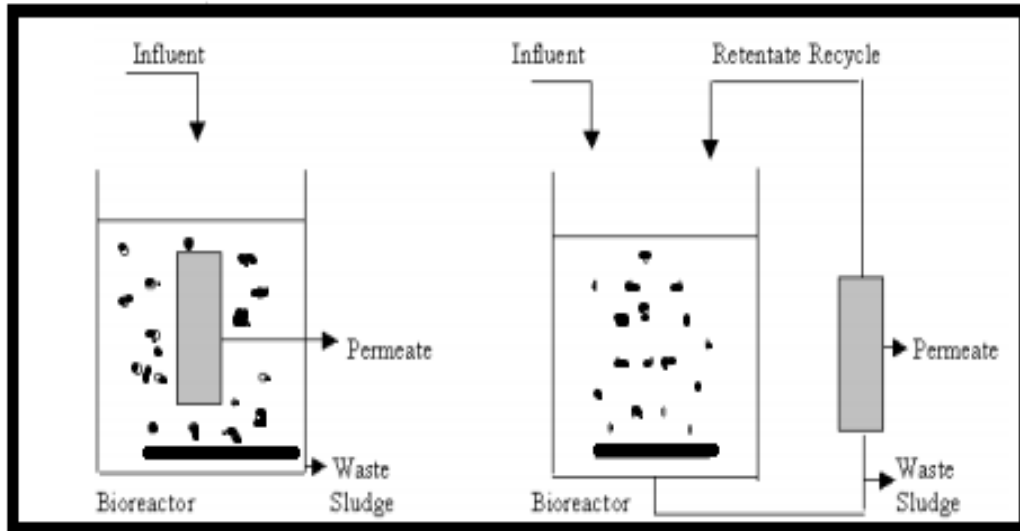
Figure 2.1: Membrane Bioreactor System

2.2.5   *Activated Carbon*

Removal of synthetic and natural organic contaminate have long been attained by use of activated sludge. Packed bed filter is used to support powder or pellet form the activated carbon. Phenomena of adsorption and filtration are simultaneity used in granular activated carbon. Regeneration of adsorbent and environmental problem are main concerns for this process [82]. Biological activate carbon used the coupled effect of adsorption and biodegradation to purify water. For such process activate carbon work as carrier. Carrier activated carbon major role is to accumulate the friendly microorganism on its surface such that a number of microorganism get accumulate on activated carbon[83]. This is done by providing proper parameters such as temperature and nutrient on surface of activated carbon to allow the suitable and friendly microorganism grown on surface of activated carbon. Due to favorable condition microorganism can useful grown and reproduce on surface of activated carbon. Such a combination will exert combined effect of adsorption

and biodegradation due to action of activated carbon high surface area and bio action of microorganism respectively. Activated carbon can adsorbent dissolved oxygen on its surface and microorganisms will grow on this dissolved oxygen. Such a combination will destroy and degrade pharmaceutical and bio organism harmful to water purification. [84, 85].

2.2.6 *Disinfection by Ozonation*

The decomposition of ozone in water gives radical i.e., OH, and hydrogen peroxide. Both species have great oxidation capability. It is extremely important to the disinfection of water process. Bacteria are killed by because of protoplasmic oxidation of ozone [86]. The efficiency of disinfection process depends upon probability of target pathogen, pharmaceuticals. The feed gas source for the ozone generator is air or pure oxygen, which is fed through it at a set flow rate. Electrical discharge or electrical energy is used to create ozone by passing current through the oxygen [87]. After generation of ozone, it is used as feed inside the wastewater chamber contain organic waste. Here sufficient time is provided for the contact of wastewater and ozone. Optimal ozone dosage is maintained for efficiency of process. Main parameters are ozone dosage, mixing and contact time. Medium to large size plant use the ozone process.[88]

2.3 Other Hybrids for Tetracycline Removal

Many researchers made hybrids of different catalysts to enhance the adsorption ability and as a result an increment in the removal of tetracycline can be seen. A researcher Hyun Min Jang et al prepare hybrid from agriculture waste (activated biochar through NaOH) for the same case and he concluded that the findings of the batch experiments showed that with its large BET surface area (796.50 m^2/g), high hydrophobicity, and pore volume (0.087 cm^3/g), NaOH-activated AF-BC (BCA) was effective at adsorbing TC in water (Q_m = 302.37 mg/g). figure 1 shows the adsorption of different catalyst used by the author [89]. Jang et al. (2018b) demonstrated a significant increase in surface area ("685.64-fold increase; from 1.4 m^2/g to 959.9 m^2/g") and Qe value for TC adsorption (9.34-fold increase; from 29.42 mg/g to 274.81 mg/g) following the NaOH activation of

pinewood virgin BC [90]. Once beetroot pulp was steam activated, lvarez-Torrellas et al. (2016) found that the Qe value for tetracycline adsorption had dramatically risen ("288.3 mg/g for steam-activated beetroot pulp BC") [91]. John Hoslett et al synthesize biochar from the food and trees trimmings in a heat pipe reactor. From his experiments he finds out that the produced biochar has outstanding ability to bind tetracycline up to 9.45 mg/g in the conditions mentioned. It was determined that the greatest explanation was given by the Freundlich isotherm., inferring a heterogeneous adsorbent. Tetracycline adsorption properties of the biochar matched those of biochar produced in similar conditions reported in previous studies. Hence, it is possible to lessen the amount of antibiotics in the environment by employing biochar produced by a heat pipe reactor utilizing agricultural waste or food/organic feedstock from residences and businesses [92].

Duanyi Zhang et al used activated carbon of high porous nature for the removal of TC from water. PAC_4 was immersed in TC solutions at different initial concentrations ("60, 75, 100, 125, 150, 175 and 200 mg/L") for his experiments. As Fig. 6 illustrates, the adsorption capacity increases significantly from 60 to 125 mg/L. As the concentration rises, the adsorption curve flattens, indicating saturated adsorption takes place. He further finds out that the absorption capability is highest at PH value of 3 and if we further increase the Ph to 7 the absorption becomes weak as as shown by figure 6. Also the a drop in the adsorption concentration occur when he increase the concentration of different salts from 0.01 to 0.1 molar [93].

2.4 Photochemical Activity
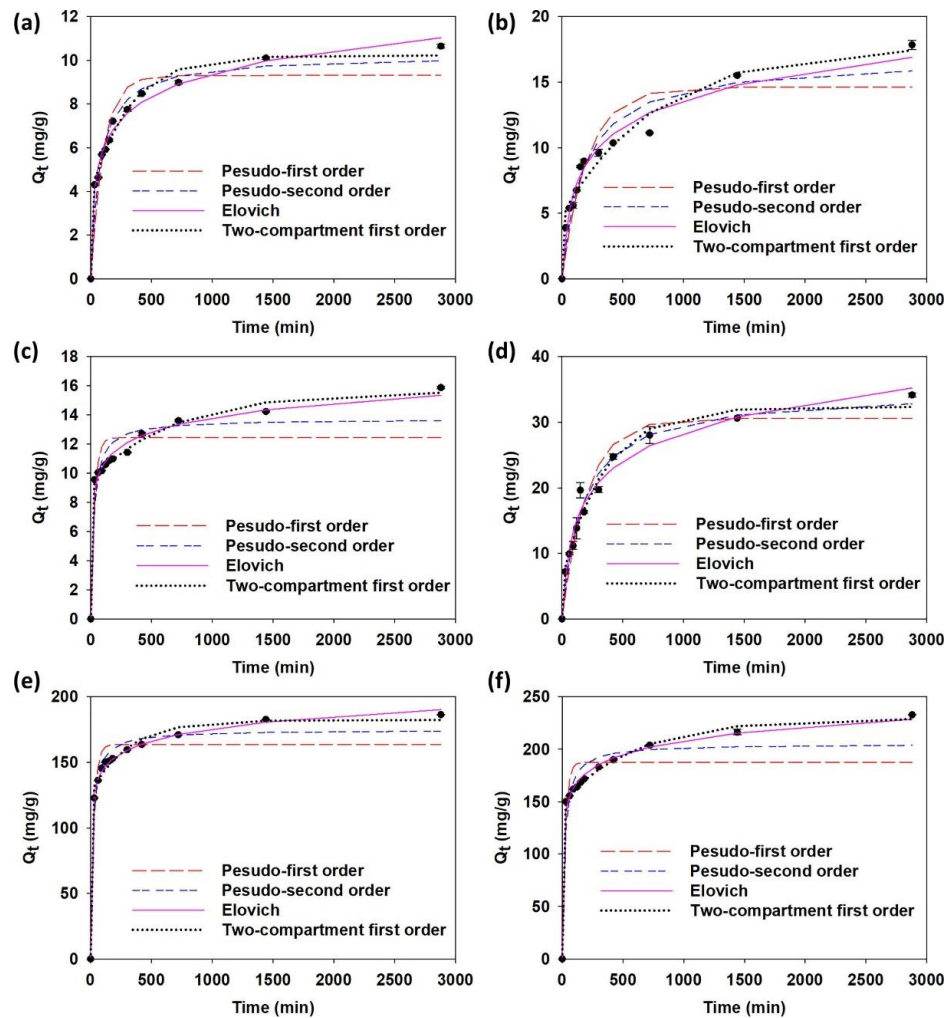
Figure 2.2: Adsorption kinetics of TC at two distinct initial concentrations for BCR
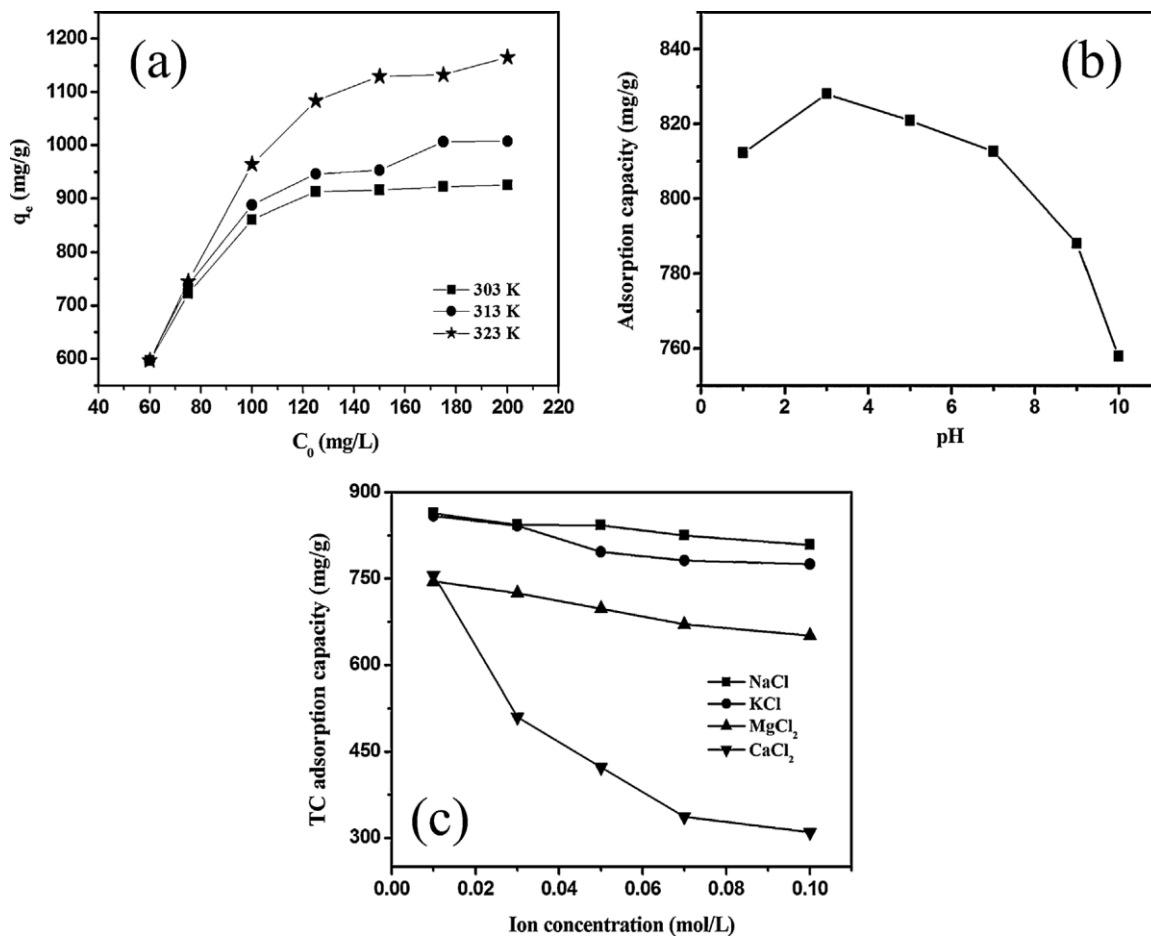
Figure 2.3: (a) Impact of initial concentration on TC adsorption, (b) impact of solution pH on TC adsorption (c) impact of solution ion strength on TC adsorption

Table 2.2: Different catalysts and their photocatalytic efficiency

S.No	Materials	Loading Catalyst	Antibiotic molecule	Condition	Photocatalytic efficiency	Times (minutes)	Reference
1	Thiourea	0.5 g/L	TC-HCl	Sunlight	70%	120	[94]
2	Melamine	0.5g/L	TC-HCl	Sunlight	63%	120	[94]

3	Urea		TYL	300 W Xe Lamp	99%	120	[95]
4	Dicyandia mide	0.5g/L	OFL	500W			[96]
5	Melamine	1g/L	TC	35 W Xe Lamp	86%	240	[97]
6	SBA-15	1 g/L	CIP	350 W Xe Lamp	92%	50	[98]
7	SiO$_2$ shell	0.33g/L	TC	300 W Xe Lamp	93%	120	[99]
8	P123-Dicyandia mide	0.5g/L	TC	300 W Xe Lamp	98%	12	[100]
9	L-cysteine	0.5g/L	SMZ	300 W Xe Lamp	99.7%	60	[101]

2.5 g-C$_3$N$_4$ as Photocatalyst

Global public health is now seriously threatened by environmental contamination due to the world's fastest-growing population and industrialization. Ever since Frank and Bard's 1977 initial report on the remediation of environmental pollutants (CN− in water) using heterogeneous photocatalysis on titania [102]. Heterogeneous photocatalysis has been extensively employed in the purification of various environmental elements, including water and air [103, 104]. Moreover, numerous strategies have been employed to raise the photodecomposition efficiency of pollutants over g-C$_3$N$_4$-based semiconductors [105]. Because of g-C$_3$N$_4$-'s special qualities—such as its enticing electronic structure, n-type semiconductor status, non-toxicity, earth abundance, and modulated band gap of 2.7 eV—it is a good option for photocatalytic water purification assisted by visible light.
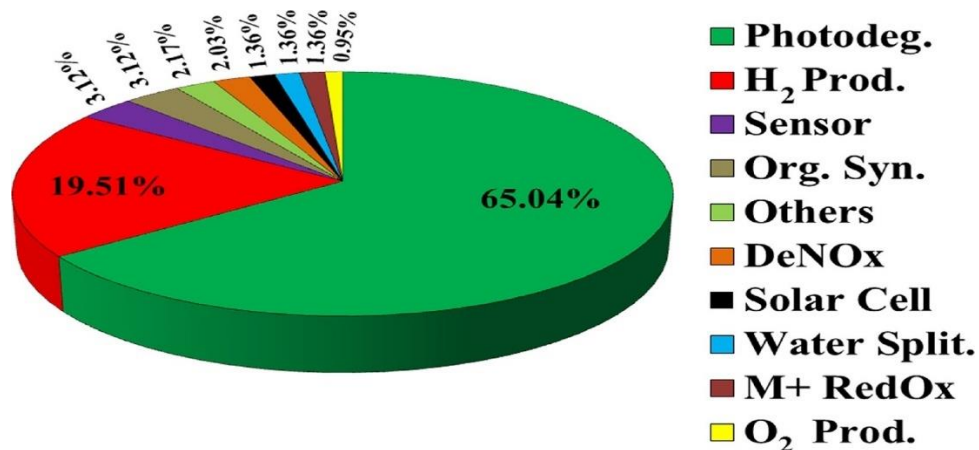
Figure 2.4: Pie chart showcasing the various photoactive uses of g-C3N4. [140]

2.6 Mechanism

2.6.1 Adsorption Mechanism, Kinetics, And Thermodynamics

Adsorption typically takes place during the water remediation process. The primary functional groups of g-C$_3$N$_4$, which are produced by directly calcining nitrogen-rich precursors, are -NH2/-NH-/=N-. By creating a heterojunction, these functional groups, as well as others like carboxylic acid and hydroxyl, can be added to enhance the adsorption efficiency for various pollutants. The adsorption mechanism of materials based on g-C$_3$N$_4$ is typically examined from two angles: (1) the way pollutants and materials based on g-C$_3$N$_4$ interact during the adsorption process; (2the adsorption process's thermodynamics and kinetics.

Typically, interactions like surface complexation, hydrogen bonding, π-π interaction, and electrostatic attraction cause the adsorption behavior between pollutants and g-C$_3$N$_4$-based materials. Surface complexation and electrostatic attraction are typically the primary interactions for the treatment of heavy metal ions and surface-charged organics; these can be verified by FTIR spectroscopy, XPS spectroscopy, and other analyses. Furthermore, one significant element influencing the adsorption efficiency of materials based on g-C$_3$N$_4$ is the pH of the solution. It was discovered that the primary cause of the cationic rhodamine B treatment with the negatively charged Cu$_2$MoS$_4$/g-C$_3$N$_4$

22

composite is the electrostatic attraction interaction. The adsorption capacity was relatively unaffected by low pH, but at pH = 9, rhodamine B's carboxylic acid groups dissociated faster and the nitrogen groups deprotonated, increasing their electrostatic repulsion and decreasing the adsorption performance [106]. The surface of the g-C_3N_4/β-CD material obtained by β-cyclodextrin modification had many functional groups and active sites (such as C double bond O, C-O-C, -OH, etc.), as indicated by FTIR and XPS spectra. The surface characteristics of g-C_3N_4/β-CD and the degree of protonation of oxygen-containing functional groups may be impacted by pH when treating Pb(II) wastewater. It may also have an impact on Pb(II)'s morphological distribution. When pH is less than 7.0, Pb^{2+} and $Pb(OH)^+$ predominate, and the primary adsorption processes involve surface complexation and electrostatic attraction between Pb(II) and hydroxyl or heptazine ring; conversely, when pH is greater than 7.0, Pb(II) primarily undergoes surface complexation with hydroxyl groups. Furthermore, the adsorption behavior of methyl orange on g-C_3N_4/β-CD was primarily attributed to hydrogen bonding and van der Waals forces [107]. Rashid et al. also discovered that the "hydrogen bonding interaction" and "π-π interaction" were the primary causes of the diclofenac adsorption by "g-C_3N_4/MoO_3". This was further supported by the "diclofenac's π-π stacking" on the nanocomposite and the propensity of -NH to increase the adsorption of diclofenac molecules [73].

2.6.2   *Photocatalytic Mechanism*

Much attention has also been drawn to the superior photocatalytic treatment performance of materials based on g-C_3N_4. To modify materials to increase photocatalytic activity and enhance wastewater treatment procedures, it is crucial to comprehend the pertinent photocatalytic mechanism. g-C_3N_4 is an n-type semiconductor that responds to visible light and possesses a "photocatalytic degradation mechanism" like heterogeneous catalysis for pollutants in aqueous solution. It consists primarily of five steps: (1) the contaminants are moved from the solution to g-C_3N_4 's surface; (2) Pollutants are adsorbed by g-C_3N_4.; (3) pollutants undergo a photocatalytic reaction on the surface of g-C_3N_4; (4) The compounds that break down are removed from the surface of g-C_3N_4.; (5) The breakdown products find their way into the solution [108].

The HOMO energy level of the nitrogen and carbon Pz orbitals is joined with the VB of g-C$_3$N$_4$. At zero energy, the higher-energy CB is empty and the lower-energy VB is fully occupied by the e- [109]. Fig. 2 depicts the "photocatalytic degradation process" of organic pollutants on the surface of g-C$_3$N$_4$. g-C$_3$N$_4$ will absorb light energy when exposed to light. The material will become excited when the energy surpasses its threshold, resulting in the production of photogenerated holes (h+) and electrons (e-). As the relatively stable electrons (e-) and holes (h+) accumulate in the valence band (VB), the electrons in the conduction band (CB) will experience an influx due to excited transitions. The electrons and holes produced by photolysis then move to the catalyst surface. Given that g-C$_3$N$_4$ has valence band potential (EVB) of about 1.3 eV and conduction band potential (ECB) of approximately 1.4 eV, respectively [110] Since the "O$_2$/•O^{2-}"redox potential is -0.33 eV relative to the normal hydrogen electrode, photogenerated electrons can readily combine with adsorbed O$_2$ molecules to produce •O^{2-}.However, compared to the "EVB of g-C$_3$N$_4$", the "•OH/OH$^-$ redox potential (+1.99 eV)" is significantly higher, meaning that the residual h+ cannot react with H$_2$O and OH$^-$ to produce •OH [111]. Nevertheless, by reducing the adsorbed O$_2$ via a "multi-electron reaction process", a tiny amount of "•OH" can still be produced [112], [108], [42]. In the end, the process can break down organic pollutants into harmless byproducts like "CO$_2$ and H$_2$O" thanks to the production of "h+, •O$^{2-,}$ and •OH".
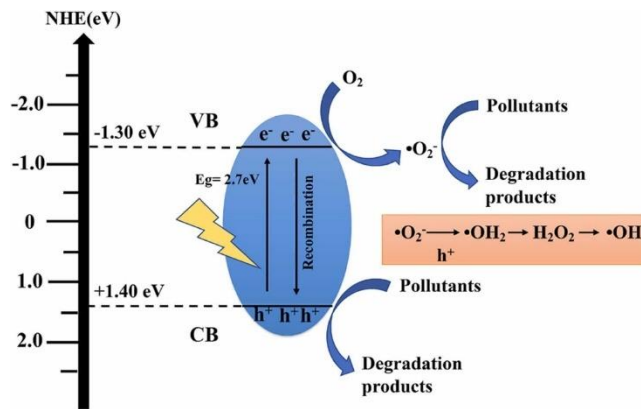
Figure 2.5: Mechanism of using g-C3N4 as photocatalyst in the photocatalytic destruction of contaminants under light irradiation [148].

2.6.3   Binary Hybrid Nan0composites

In order to overcome the application limitations of g-C$_3$N$_4$ in photocatalysis, a highly effective modification technique known as constructing binary photocatalytic systems has been introduced. In the last decade, there has been a notable surge in the investigation of "heterostructure photocatalysts" utilizing g-C$_3$N$_4$ as a base [113]. For enhanced photodegradation activity through improved spatial separation of charge carriers, it is crucial to establish suitable band structures at the interfaces between g-C$_3$N$_4$ and metal particles, inorganic semiconductors, or conducting materials. [69, 114, 115]. This indicates that the creation of heterostructures can serve as a novel approach to modifying g-C$_3$N$_4$, thereby broadening its range to incorporate new visible light-driven nanocomposites for applications in solar energy conversion and pollutant degradation.

CHAPTER 3: MATERIAL AND METHODOLOGY

3.1 Catalyst Synthesis

3.1.1 Synthesis of CdS nanorods

The synthesis of CdS nanorods involved the utilization of the solvothermal method. A mixture was prepared by combining 1.52 grams of thiourea and 3.088 grams of cadmium nitrate tetrahydrate with 50 ml of ethylene diamine. The resulting solution was continuously stirred for 10 minutes. The mixture solution was then put into a "Teflon-lined stainless-steel autoclave" and heated to 180°C for 12 hours. Subsequently, the autoclave solution was allowed to reach room temperature. Centrifugation was used to separate the resultant mixture, which was then rinsed three times with ethanol and three times with deionized water. The precipitates obtained at the end of the washing process exhibited a yellow color and were then dried in an oven for 12 hours at 80°C. Ultimately, the material that had dried was ground into fine particles.

3.1.2 Synthesis of g-C$_3$N$_4$

Using an alumina crucible and 10 grams of melamine, the synthesis of g-C$_3$N$_4$ was initiated. After that, this crucible was heated in a muffle furnace to 550°C and kept there for three hours. It was then allowed to cool naturally. A light-yellow precipitate of g-C$_3$N$_4$ was produced during the cooling process, and it was later ground into a fine powder.

3.1.3 Synthesis of ZIF-67

The "solvothermal" method was employed in the synthesis of "ZIF-67". 50 milliliters of methanol were used to dissolve 0.656 grams of "2-methylimidazole" and 0.585 grams of "cobalt nitrate hexahydrate" in separate beakers. For ten minutes, magnetic stirring was applied to each solution. Both solutions were then combined and agitated for a further thirty minutes. The resulting mixture was left to age for a duration of 72 hours.

After this aging period, the solution was subjected to vacuum filtration using a nylon filter membrane. This process yielded purple-colored precipitates of ZIF-67.

3.1.4 Synthesis of g-C₃N₄@CdS

To synthesize g-C$_3$N$_4$@CdS hybrid, the solvothermal method was employed. Initially, 5 mg of the as-synthesized pure g-C$_3$N$_4$ catalyst was introduced into 50 ml of ethylene diamine and agitated for half an hour. Following this, a solution mixture was prepared by adding 3.008 grams of cadmium nitrate tetrahydrate and 1.52 grams of thiourea to the g-C$_3$N$_4$-ethylene diamine solution, which was then stirred for 10 minutes. The resultant mixture was then put into a "Teflon-lined stainless-steel autoclave" and heated to 180°C for 12 hours. After the heating process, the solution in the autoclave was permitted to cool down to ambient temperature. Centrifugation was used to separate the resulting mixture, which was then rinsed three times with ethanol and washed three times with deionized water. Yellow-colored precipitates obtained at the end of the washing procedure were dried for a while at 80°C. 12 hours in an oven. The dried material was then finely ground into fine particles. The same experimental procedure was repeated for 10 mg and 15 mg of g-C$_3$N$_4$ to synthesize hybrids with CdS.

3.1.5 Synthesis of CdS@ZIF-67

To synthesize a CdS hybrid with ZIF-67, the solvothermal method was employed. Initially, 5 mg of CdS was added and agitated for ten minutes in 50 milliliters of methanol. Following that, 0.656 grams of 2-methylimidazole were combined with the same mixture and agitated for an additional 10 minutes. In a separate beaker, 50 milliliters of "methanol" were used to dissolve 0.585 grams of "cobalt nitrate hexahydrate", and the mixture was also stirred magnetically for ten minutes. Following that, both solutions were integrated and further stirred for half an hour. The resulting mixture was left to age for a period of 72 hours. Following this aging period, the solution was subjected to vacuum filtration using a nylon filter membrane. This process yielded purple-colored precipitates of the CdS@ZIF-67 hybrid. The same experimental procedure was repeated for 10 mg and 15 mg of CdS to synthesize hybrids with ZIF-67.

3.2   Characterization Techniques

The STOE GERMANY diffractometer was used for "X-Ray Diffraction" (XRD) analysis, utilizing copper (Cu) material with kα radiation and a wavelength of 1.5406 Å. The purpose of XRD was to identify the catalyst by examining its diffraction pattern. The catalyst's morphology was examined using "scanning electron microscopy" (SEM) with the JEOL JSM-64900 device. Prior to SEM characterization, a thin conductive layer of gold was applied through sputter coating onto the catalyst and its respective hybrids. To examine photocatalytic activity and degradation, a Cary-100 BIO UV-VIS spectrophotometer was utilized.

3.2.1   SEM

Sample details can be obtained with a scanning electron microscope, or SEM, which is widely studied. It consists of a beam of light. The electrons that make up the SEM beam have a tremendous amount of energy. This beam is applied to the sample surface. In this manner, the sample's structural aspect is disclosed.

An electron beam creates specific features on the material's exterior. The information about the morphology of the sample is transferred using data analyzers. Most of the data is collected inside and outside of the sample's designated range. This device is used to examine and comprehend desired points across the sample's exterior. The SEM's potential is functional like that of the probe electron microscope. By correctly using SEM, morphological and topological features of the sample can be investigated. We're able to SEM can reveal the dimensions, surface and bulk properties, and shape of the sample. When the SEM's light beam incidence causes a difference in the kinetic energy of the incident and transmitted electrons during this process. An image of the sample under investigation is created because of numerous electrons being scattered and secondary electrons being produced. The topography, shape, and other relative features of the samples are revealed by this phenomenon. The influence of the second electron is what causes phase differences. The interaction between an electron in the sample's orbit and an electron in the SEM's striking beam produces X-ray radiation.

3.2.2   XRD

XRD can provide information about the sample's crystallites. It provides important details about the sample. Important characteristics that this machine reveals include crystallography, size of crystal, and Miller indices. Though smaller than UV, X-ray wavelengths are larger than Y-ray wavelengths. In comparison with x-rays, UV-rays have weaker photon energy, whereas Υ-rays have higher photon energy in relation to x-rays. The wavelength magnitude of x-rays is 1 Å. XRD is based on the idea that electron transitions occur because of an electron striking a metal. Copper or molybdenum are the target metals used to generate X-rays. Ionization happens when a metal is exposed to radiation because electrons are emitted from its internal shell or because this process knocks electrons out of their orbits. Therefore, the knocking phenomenon causes a void to form in the metal's orbit. An electron in an orbital with a higher energy and position than the orbital of the knocked-out electron will attempt to fill the void. This falling electron will release radiation that can be used to accomplish the goal, specifically X-rays.

A thorough mathematical relationship called Bragg's law is used to effectively explain the diffraction phenomenon. It is frequently used in diffraction of crystals. FWHM and crystallite size are determined with the help of data provided by Bragg's law. Any distinct crystalline material subjected to X-ray diffraction (XRD) will produce a specific characteristic X-ray spectrum.

3.2.3   UV-Vis Spectrophotometery

We use spectroscopic measurement equipment, also known as UV-Vis spectroscopy, to examine the sample's response to the application of the visible and ultraviolet ranges of the electromagnetic spectrum. Every material has a unique molecular configuration, with functional groups that have distinctive UV-visible absorption edges. Information about the material's UV-vis response is displayed when a difference in absorption occurs. Using this method, minute pollutants in a solution are revealed.

Peaks that differ from the material's are providing information about the contaminants. It can be used to monitor the continuous profile of a chemical reaction. For

instance, it is highly suitable for uninterrupted analysis of the photocatalytic removal process's progress. The foundation for the quantitative analysis of solution behavior using UV-VIS is the Beer-Lambert law.

Variations in the specimen's UV-vis behavior during the investigation will reveal the spectrum produced by the UV-Vis spectrometer. This spectrum is compared to previously identified and computed spectrums. Certain wavelength ranges have absorption edges for distinct functional groups. When there is a chance that an atom contains pie or non-binding electrons, electrons are excited to higher orbitals. since UV-Vis light interacts with these electrons. Ultraviolet-visible spectrophotometers have been used in many experiments recently. In comparison with chemical reaction reagents, it offers an easier process. This procedure makes it simple to investigate adsorption experiments. By using this technique, different reactions that arise from the adsorption of both organic and inorganic dye on the adsorbent surface can be studied. Furthermore, photocatalysis reactions are frequently performed using the appropriate technique. The dye and pollutant exhibited a sharp trend by responding differently to the light from the UV-Vis spectrometer.

Using this method, the kinetics of dissolution of various polymers and sand-coated composites were examined. This method can be used to predict both the speed and slowness of a reaction. When examining first order, second order, and pseudo order reactions, this approach is highly helpful. The reaction parameter is easily found by closely plotting the data. UV-vis radiation analysis is a useful tool for chemical engineers looking to design reactors efficiently. Ultimately, this will assist the research student in identifying the weaknesses in reaction monitoring when using chemical reaction engineering in research methodology. Today's modern laboratories are well equipped with this type of technique to qualitative and quadrative investigate the reactor feature. When the difference between HOMO and LUMO is much low. In such scenario low energy is attained form HOMO for transition to happen to higher state which is also called as LUMO. The longer wavelengths of radiation are what cause the excitation because they have a specific energy that allows them to do so. When the gap between the HOMO and LUMO is equivalent to a band gap-sized packet of photons, electrons migrate from the HOMO to the LUMO. The

term "σ - σ*" refers to this type of electron transfer (nonbonding sigma to bond sigma molecular orbital). Cuvettes are used in UV-VIS spectroscopy to reveal sample behavior. In this process, two types of cuvettes—quartz and glass cuvettes—are utilized. Economically speaking, quartz is very costly, has very little transmittance loss, and is highly specialized. The UV-vis machine belongs to multiple classes. Both single and double beams are present. There is only one reference point made in a single beam. In contrast, double beam makes use of two standard mixture references and measurements.

3.3   Photocatalytic Experiment

Photocatalytic experiments were conducted to assess pure CdS, ZIF-67and g-C$_3$N$_4$ their nanohybrids' photocatalytic activity using a 100 mg/L tetracycline solution at room temperature. A bottleneck flask was filled with 1000 mL volume deionized water and 100 mg of tetracycline was added, followed by stirring for half an hour to ensure a homogeneous mixture. 100 mg of the corresponding catalyst was added to a beaker containing 100 mL of the solution. To maintain complete darkness, aluminum foil was used to wrap the beaker. After that, the mixture was continuously stirred for 30 minutes while being stored in a wooden box to accomplish the equilibrium between "adsorption and desorption". After 30 minutes, the photocatalytic reactor bulb was turned on to start the photocatalytic process. The overall duration of the degradation experiment was 210 minutes. At 20-minute intervals, samples were collected using a syringe equipped with a nylon filter at the tip. For the degradation analysis of the tetracycline solution, characteristic peaks at 275 nm and 350 nm were monitored using a UV-Visible spectrophotometer. These peaks corresponded to tetracycline.

CHAPTER 4: RESULTS AND DISCUSSION

4.1 XRD Analysis

The STOE θ-θ diffractometer was operated with a 40-mA power supply and 45 kV to analyze crystallography and phases of the samples. The instrument utilized a copper anode to generate fluorescence (kα radiation with λ=1.5406 Å) for phase analysis. The range of the XRD angle (2θ) was 10 to 80 degrees. XRD patterns for pure g-C3N4, pure CdS, and their hybrids are exhibited in the respective figures, while XRD patterns for Pure ZIF-67, pure CdS, and their hybrids are shown in the corresponding figures.
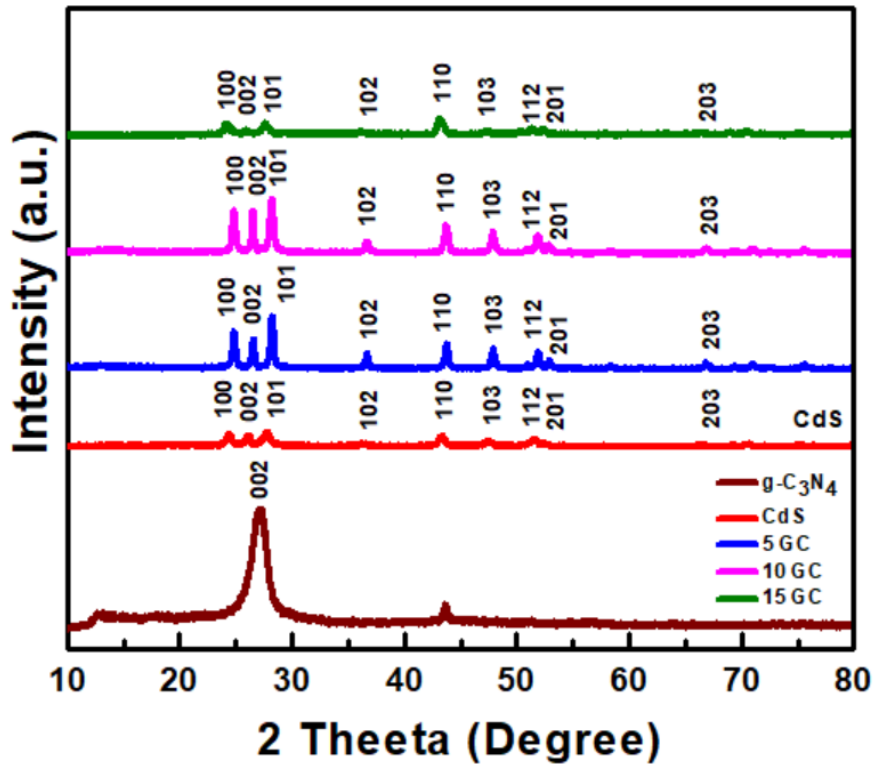

Figure 4.1: XRD pattern of pure CdS, pure g-C3N4, and their hybrids (5 mg, 10 mg, and 15 mg) g-C3N4@CdS.
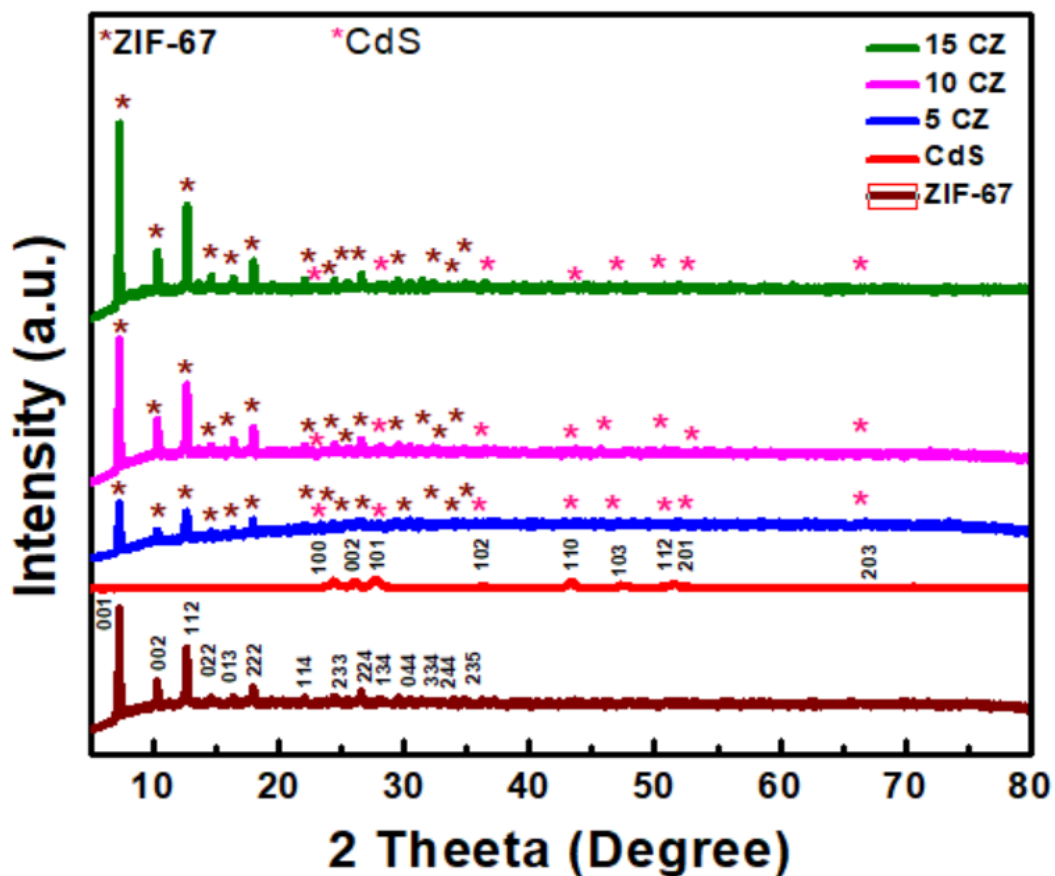
Figure 4.2: XRD Pattern of pure ZIF-67, pure CdS, 5 mg CZ, 10 mg CZ & 15 mg CZ.

X-ray Diffraction (XRD) analysis was employed to ascertain the crystalline structure of our synthesized samples and evaluate their degree of crystallinity, whether they exhibited a crystalline or amorphous nature. Figure 10 (i) presents XRD patterns of pure "graphitic carbon nitride" (g-C_3N_4), pure "cadmium sulfide" (CdS), and their prepared hybrids at various weight percentages. In Figure (a), the XRD pattern of Pure g-C_3N_4 clearly exhibits characteristic peaks of g-C_3N_4 at a 2θ value of 27.4, corresponding to the (002) plane. This peak aligns with JCPDS card number 87-1526, as documented in the literature. Figure (b) displays the XRD pattern of pure CdS, revealing peaks on planes (100), (002), (101), (102), (110), (103), (201), and (203) at 2θ positions of 24.7, 26.2, 28.089, 36.33, 43.6, 47.44, 50.8, and 66.4, respectively. These peaks are consistent with

hexagonal cadmium sulfide, as per JCPDS card number 41-1049, which corroborates previous findings in the literature. Figures (c), (d), and (e) represent the XRD patterns of CdS and g-C_3N_4 hybrids. In these hybrid patterns, all the characteristic peaks of pure cadmium sulfide are visible at 2θ values of 24.7, 26.2, 28.089, 36.33, 43.6, 47.44, 50.8, and 66.4, corresponding to planes (100), (002), (101), (102), (110), (103), (201), and (203).

Additionally, the prominent peak of g-C_3N_4 at 2θ value 27.4 on the (002) plane merges with the peak at the same position and plane as cadmium sulfide. This confirms the successful synthesis of the prepared hybrid. Moreover, from these peaks, it is evident that CdS dominates the hybrid, as it completely suppresses the g-C_3N_4 particles, corroborated by SEM images. Figure 3 (ii) illustrates the XRD patterns of ZIF-67 hybrids with CdS. In Figure (f), the XRD pattern of Pure ZIF-67 displays peaks at 2θ values of 7.33, 10.348, and 12.687, corresponding to planes (110), (200), and (211). These peaks align with JCPDS card number 01-089-2803, as also observed in literature. Patterns (h), (i), and (j) show the XRD patterns of the hybrids of ZIF-67 with CdS. In these hybrid patterns, prominent peaks of ZIF-67 are visible on planes (110), (200), and (211).

Importantly, there are no discernible peaks of CdS in these hybrids, indicating that the cadmium sulfide particles have penetrated the pores of ZIF-67. This is further confirmed by SEM images. The crystal sizes of all the fabricated catalysts were calculated using the Scherrer formula and are presented in Table 3. Notably, the hybrid exhibited a smaller crystal size, which contributes to its superior activity compared to all the prepared catalysts.

Table 4.1: Average crystal size of all the prepared samples

Photocatalyst	FWHM	Peak Position	Crystal Size	Average Crystal Size	(nm)

ZIF-67 (Pure)	0.3311, 0.138, 0.661, 0.386	10.183, 12.330, 21.778, 26.234	247,615,124,216	307.25	30.725
CdS (Pure)	0.510, 0.364, 0.665, 0.510	24.352, 26.146, 27.070,43.354	162, 229,126,170	171.75	17.175
10 mg g-C_3N_4@CdS	0.255, 0.218, 0.255, 0.255	24.352, 26.146, 27.070,43.354	329, 388, 331, 346	348.5	34.85
5 mg g-C_3N_4@CdS	0.378, 0.378, 0.315, 0.220	24.083, 25.945, 27.536, 43.045	220,220, 266, 403	277.25	27.725
g-C_3N_4 (Pure)	0.756, 0.378, 0.307	12.669, 26.945, 43.635	107, 221, 286	204.67	20.467
	0.146,0.146, 0.109,0.109	7.287, 10.329, 12.665, 17.973	577,578,791,796	685.5	68.55
15 mg g-C_3N_4@CdS	0.301, 0.167, 0.355, 0.201	24.781,26.500, 28.215,43.722	278, 513, 236, 444	367.75	36.775
5 mg CdS/ZIF-67	0.146,0.146, 0.182, 0.109	0.138, 0.138, 0.174, 0.101	577, 578, 459, 796	602.5	60.25
10 mg CdS/ZIF-67	0.109, 0.146, 0.109,0.109	7.291, 10.303, 12.652, 17.971	788,578, 791, 796	738.25	73.825
15 mg CdS/ZIF-67	0.100,0.100, 0.100, 0.100	7.291, 12.303, 12.652, 17.971	865, 867, 869, 874	868.75	86.875

The average crystallite size of ZIF-67 (Pure), CdS (Pure), 10 mg g-C₃N₄@CdS, 5 mg g-C₃N₄@CdS, g-C₃N₄ (Pure), ZIF-67 (Pure), 15 mg g-C₃N₄@CdS, 5 mg CdS/ZIF-67, 10 mg CdS/ZIF-67, and 15 mg CdS/ZIF-67 is 307.25Å (30.725nm), 171.75Å (17.175nm), 348.5Å (34.85nm), 277.25Å (27.725nm), 204.67Å (20.467nm), 685.5Å (68.55nm), 367.75Å (36.775nm), 602.5Å (60.25nm), 738.25Å (73.825nm), and 868.75Å (86.875nm) respectively.
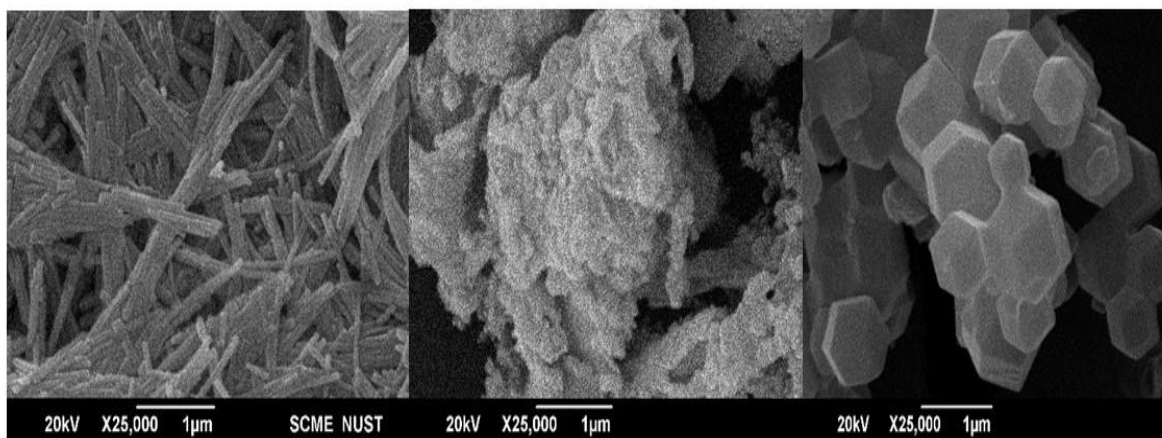
4.2 Morphological Analysis with Elemental Analysis

Figure 4.3: SEM images of pure CdS, g-C3N4 and ZIF-67 respectively.

Morphological characteristics of fabricated catalyst was examined using a scanning electron microscope (SEM) from "JEOL (JSM-64900)". Before SEM analysis, the samples underwent sputter coating with a thin conductive layer of gold. SEM imaging of "g-C3N4, ZIF-67, CdS, g-C3N4/CdS, and CdS/ZIF-67" hybrids are presented. In figure (a), CdS-NRs are depicted with a rod-like structure featuring consistent dimensions and a flat surface. On higher resolution Nano rods stacked, against each other are evident. This is possibly because of nucleation and growth of crystals. Moving to Figure (b), the SEM image exhibits morphological structure like flakes/lamellar sheets of pure g-C₃N₄, revealing porous structures with a notably high surface area. These stacking layers suggest similarity of g-C₃N₄ with graphite which is analogous of g-C₃N₄. Figure (c) showcases

36

well-defined cubic structures of ZIF-67. It shows rhombic dodecahedron crystals of ZIF-67 with smooth surfaces, clear edges and properly defined facets. Nano size crystal of as synthesized ZIF-67 was well separated from each other and there was no agglomeration.
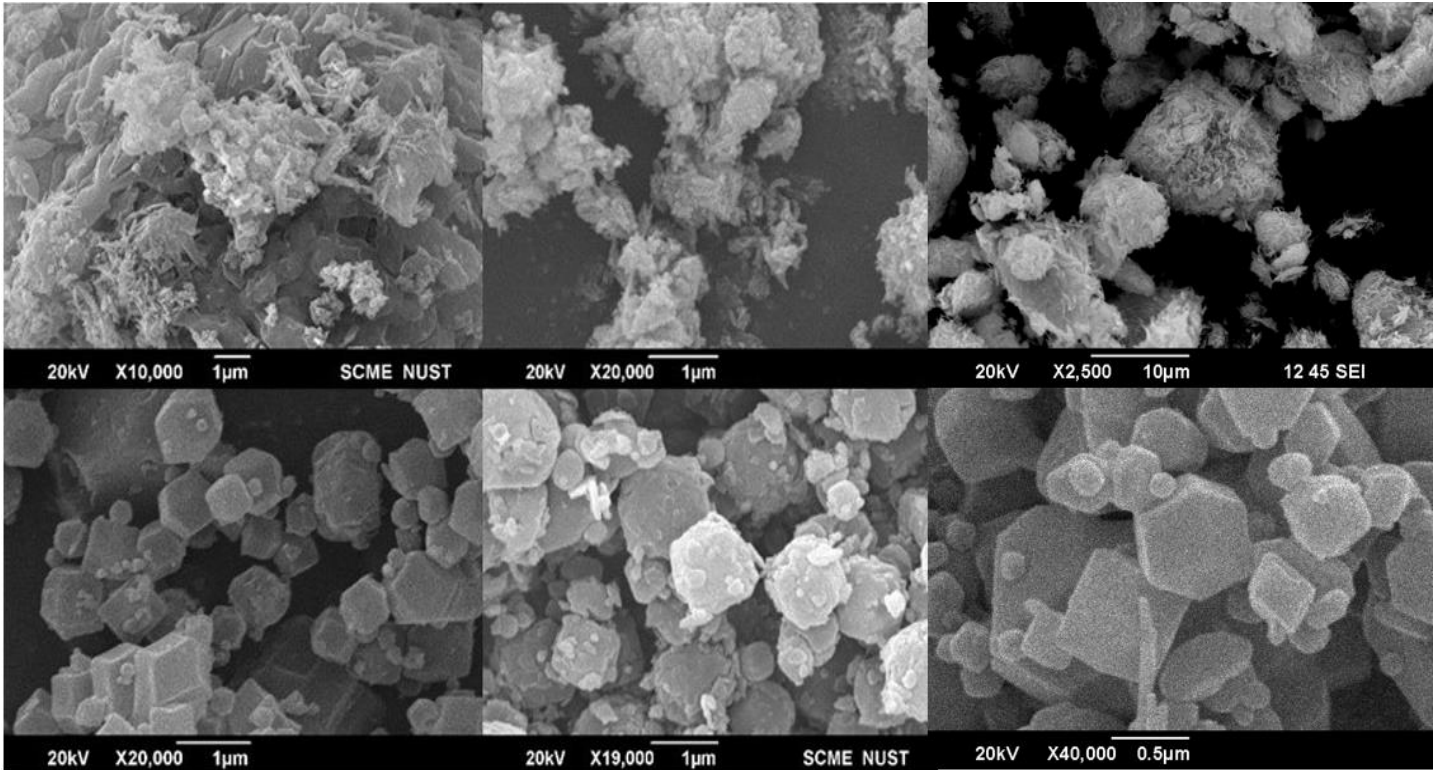
Figure 4.4: SEM images of hybrids composed of g-C3N4 and CdS (d-f), and hybrids of CdS and ZIF-67 (g-i)

Scanning electron microscopy (SEM) is used to examine the morphology of CdS-NRs (Cadmium Sulfide Nanorods) and their hybrids with $g-C_3N_4$ and ZIF-67. Figures (d)-(f) present SEM images of hybrids composed of CdS and $g-C_3N_4$ and are clear manifestation of morphological characteristics of in situ grown sheets of $g-C_3N_4$ in CdS nanorods. In all these images, a uniform distribution of CdS nanorods can be observed alongside $g-C_3N_4$ nanosheets. Graphitic carbon nitride's presence has expanded the surface area, creating more interconnecting layers of $g-C_3N_4$ and exposing additional active sites of CdS. Similarly, Figures 7(i)-(k) represent SEM images of hybrids formed by combining

37

CdS with ZIF-67. In these figures, we clearly observe the growth of CdS rods on the cubic structures of ZIF-67, confirming the successful synthesis of these hybrids. The rhombic dodecahedron-shaped crystals of ZIF-67 exhibit a uniform distribution across the surface of CdS nanorods, likely attributed to the sonication process of CdS in a ZIF-67 solution. Additionally, structures resembling rod-like CdS with incorporated ZIF-67 are observed. ZIF-67 effectively envelops the nanorods of CdS from all sides, edges, and surfaces, resulting in a smooth appearance of the CdS rods. Nanorods of CdS can be clearly seen on high resolution. Furthermore, the activity of these hybrids is enhanced because of the resultant particles' larger surface area. As the amount of CdS increases, the cubic structures of ZIF-67 become more extensively covered by rods, leading to a corresponding increase in activity. ZIF-67, g-C$_3$N$_4$ and CdS appear under SEM comparable to literature when seen as individual components. However, appearance in hybrid is different.
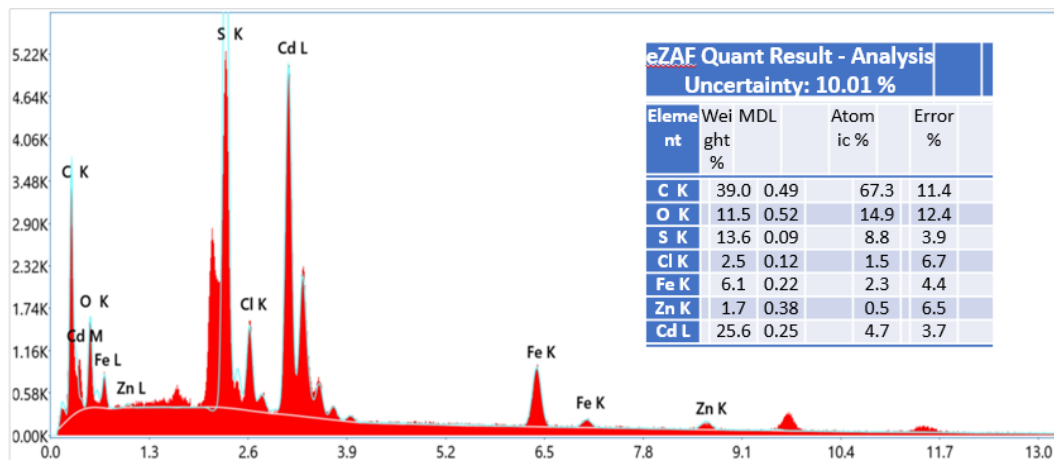

Figure 4.5: EDX of CdS Catalyst

Energy Dispersive X-ray (EDX) is performed to confirm that synthesized catalyst has all the necessary elements.
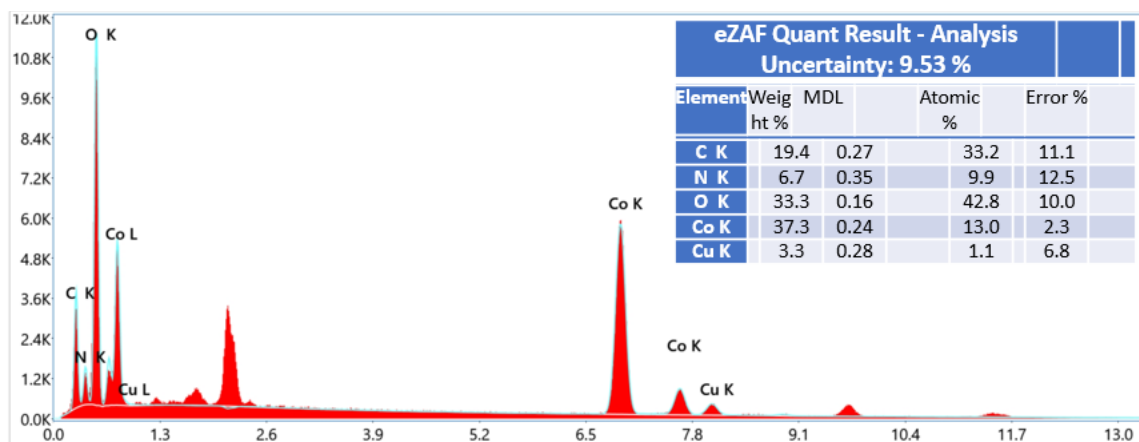
Figure 4.6: EDX of ZIF-67

4.3 Photocatalytic Degradation of Tetracycline

4.3.1 Kinetic Study of Reactions

Figures 15(a-c) display the absorbance spectra of tetracycline over time in the presence of photocatalysts 5CZ, 10CZ, and 15CZ, respectively. The CZ catalyst was synthesized by maintaining a constant ZIF-67 concentration and varying the CdS concentration, resulting in 5 mg, 10 mg, and 15 mg CdS for 5CZ, 10CZ, and 15CZ, respectively. A 100 mg catalyst was introduced into the tetracycline solution. To reach adsorption equilibrium, for thirty minutes, the solution was kept in the dark. Characteristic peaks of tetracycline reached saturation values. Afterward, 2 ml of the solution was taken out of the beaker to measure UV absorbance, and then the lamp was turned on. Among these, 15CZ emerged as the most effective catalyst, exhibiting a remarkable 96.13% removal of tetracycline within 110 minutes using only 100 mg of the nanohybrid.

The degradation of tetracycline is primarily governed by both photocatalysis and adsorption mechanisms. A significant portion of degradation takes place within the first 30 minutes. Following this period, CZ begins to absorb photons of light, leading to a rapid degradation owing to its photoactive properties. In total, CZ effectively eliminates 96.13% of tetracycline, surpassing all other synthesized catalysts. Type 2 heterojunction formed on

ZIF-67 could be the reason for high removal of tetracycline by 15CZ. Adsorption enhancement in initial 30 mins contributes to overall photocatalytic degradation.

High degradation up to 96.13% is due to enhancement in meso-porosity and high number of active sites on the surface of 15CZ for augmented pie-pie interaction between the tetracycline and 15CZ. For 5CZ and 10CZ, the percentage removal was 80.08% and 89.5%, respectively. Notably, 15CZ exhibited a dual role as both a proficient adsorbent and an excellent photocatalyst. It acted as a good adsorbent by removing nearly 40% of tetracycline within the first 30 minutes in the dark. Simultaneously, it proved to be the best photocatalyst, achieving the highest percentage removal of tetracycline in 110 minutes compared to the other catalysts. In the presence of light, CZ nanohybrids demonstrated the highest tetracycline removal efficiency.

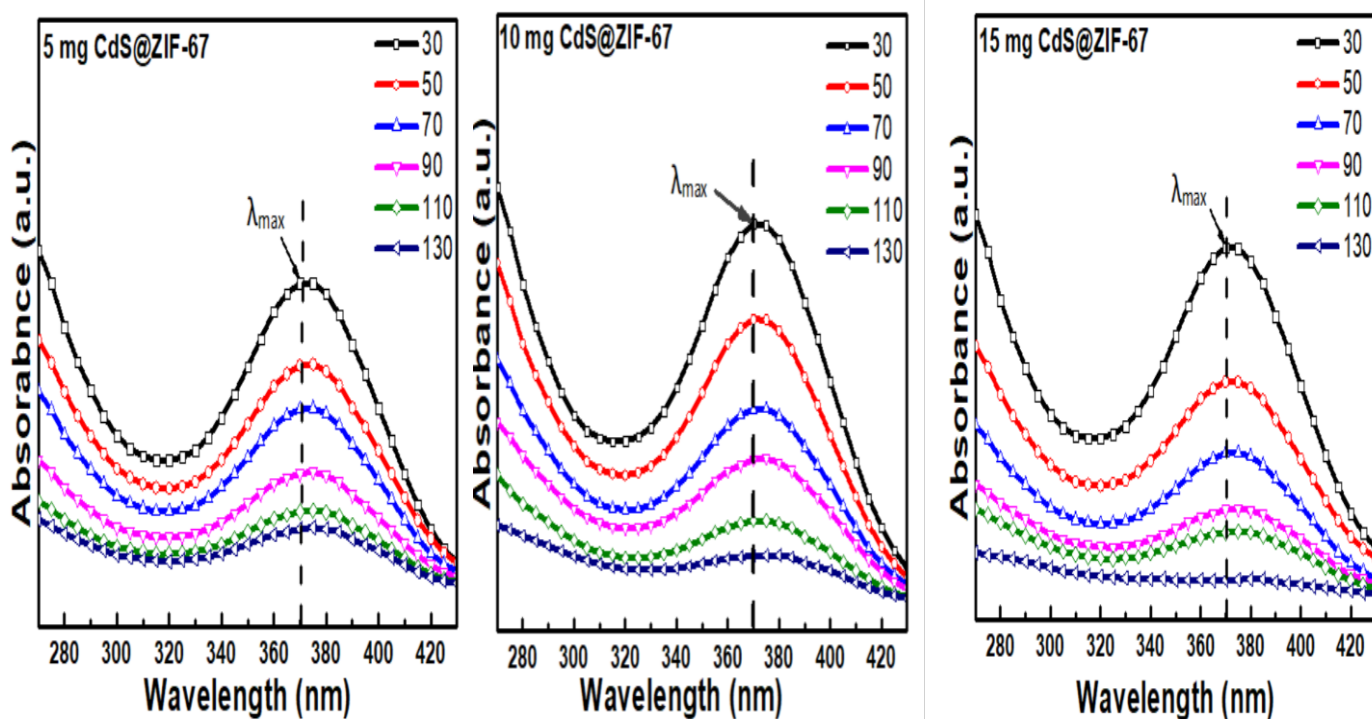

Figure 4.7: Photocatalysis by 5mg, 10mg and 15mg CdS@ZIF-67

Peaks at 275nm and 357nm degrade significantly because of possible interaction of A and BCD ring of tetracycline molecule. Saturation of peaks is achieved in both of peaks.

Figure 16(d-f) depicts the absorbance spectra of tetracycline over time in the presence of photocatalysts 5GC, 10GC, and 15GC, respectively. The GC catalyst was synthesized by maintaining a constant CdS concentration while varying the g-C$_3$N$_4$ concentration, resulting in 5 mg, 10 mg, and 15 mg of g-C$_3$N$_4$ for 5GC, 10GC, and 15GC, respectively. A 100 mg catalyst was introduced into the tetracycline solution. Subsequently, 2 ml of the solution was taken out of the beaker to measure UV absorbance, followed by turning on the lamp. In Figures y(a-c), a noticeable decrease in absorbance can be observed, indicating the ability of the GC catalyst to degrade tetracycline, as absorbance decreases over time.

Among the GC catalysts, 15GC exhibited the highest tetracycline removal rate, achieving a remarkable 90.7% removal within 110 minutes using only 100 mg of the catalyst. The other catalysts, 5GC and 10GC, achieved percentage removals of 82.4% and 89%, respectively. Additionally, 15GC demonstrated proficiency as an adsorbent, removing nearly 35% of tetracycline within the first 30 minutes.
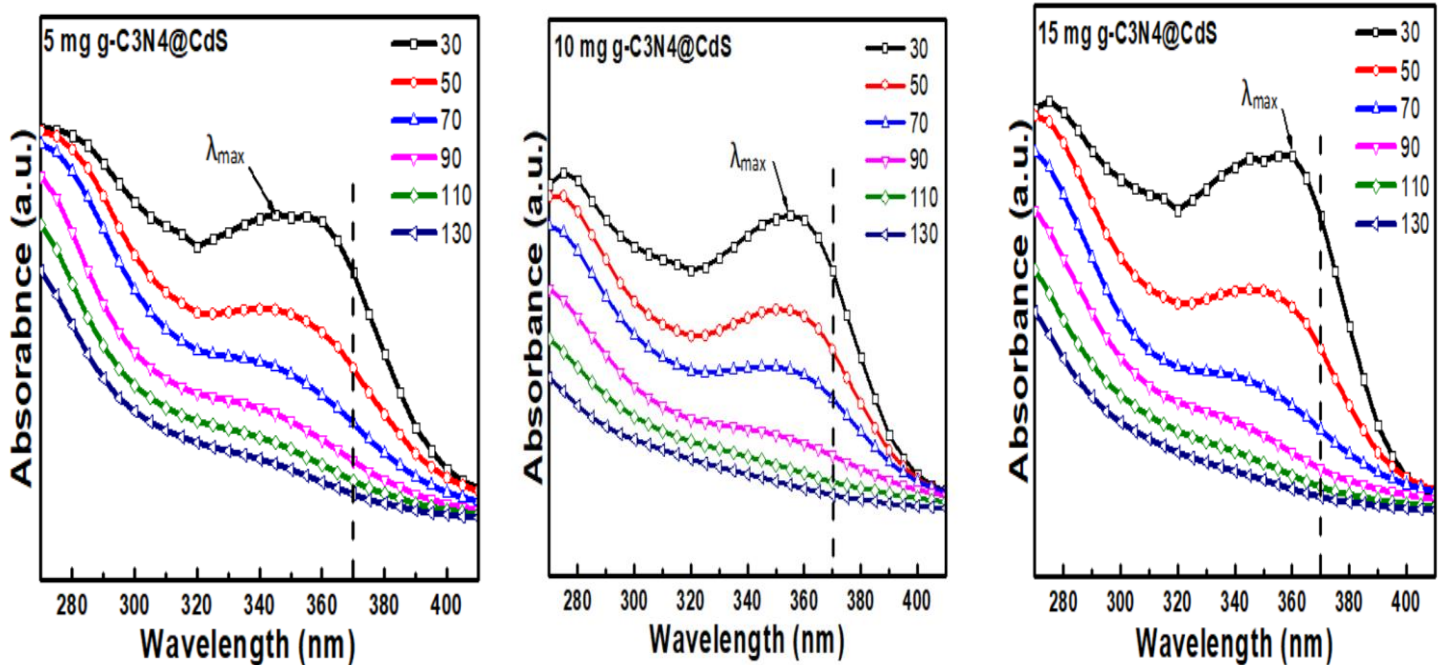

Figure 4.8: Photocatalysis by 5mg, 10mg and 15mg g-C$_3$N$_4$@CdS

Shown in Figure, the tetracycline peak at 350nm quickly reaches saturation, indicating that g-C$_3$N$_4$ exhibits excellent photocatalytic activity. It indicates that peak at 350nm degradation occurs because of possible interaction of electrons and holes with the BCD rings system of tetracycline molecule.

Possible degradation mechanism does not involve any complex mechanism of heterojunction. Rather GC can be considered photoactive due to presence of narrow band gap semiconductor material g-C$_3$N$_4$ onto adsorbent material CdS.

Tetracycline molecules first get adsorbed onto the surface of CdS and then get degraded by hole and electrons generated on surface of g-C$_3$N$_4$ due to band gap transition between nitrogen and carbon in heptazine unit of g-C$_3$N$_4$. The percentage removal of tetracycline was computed utilizing the formula [{(C$_o$-C)/C} *100].

$$Percentage\ Removal\ of\ Tetracycline = \frac{C_0 - C}{C} \times 100 \qquad (4.1)$$

Where C is the concentration at the specified time and C$_o$ represents the initial concentration. As the concentration of g-C$_3$N$_4$ in the nanohybrid increased, there was an increase in the percentage removal of tetracycline correspondingly.

g-C$_3$N$_4$ is a highly effective photocatalyst with high photostability and minimal charge carrier recombination. As a result, obtaining the required properties in the nanohybrid depends critically on its optimum concentration.

The mesoporous structure of "g-C$_3$N$_4$", "ZIF-67", and "stacked nanorods of CdS" contributes to the adsorption of TC onto the catalyst surface in all hybrids. The exposure to incident light further enhances the degradation of TC.

During the photocatalysis carried out by hybrids, both peaks are reduced in intensity till saturation is achieved. Maximum percentage removal is shown by 15CZ with a value of 96.13%.
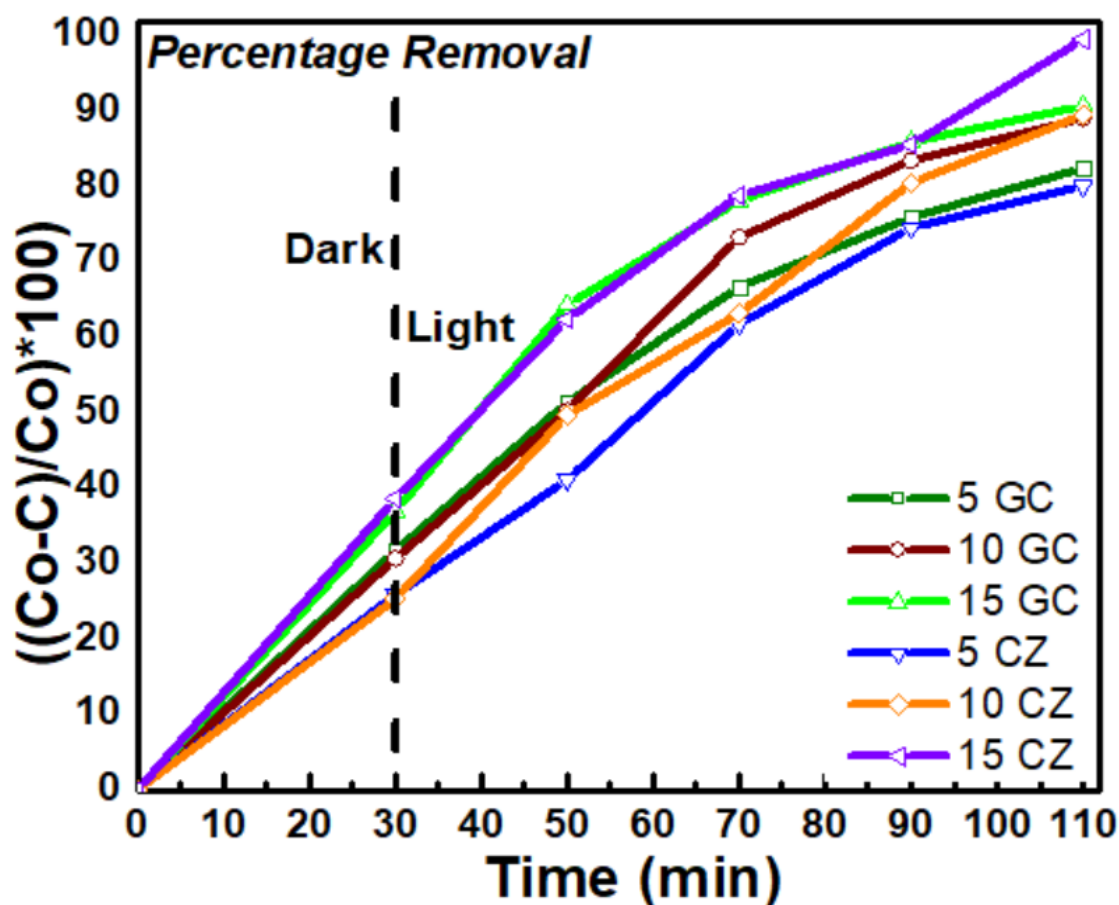
Figure 4.9: Percentage removal of tetracycline by all synthesized hybrids.

The reaction kinetics of catalyst was investigated under fixed temperature as shown in figure. The rate of the reaction exhibited a significant reliance on the adsorption of solute onto the surface of the photocatalyst. Light intensity of reactor has also increased reaction rate due to absorption of photons by photo catalyst.

Reaction kinetics was studied by plotting $\ln(C/C0)$ versus time as shown. All reactions follow pseudo first order fit with R^2 values greater than 0.90. In Figure 15, the kinetic model of the reaction is presented. The analysis of the kinetics of the tetracycline decomposition reaction involved fitting the kinetic model to determine the reaction kinetics and 1st order rate model. The "rate constant" (k) and order (n) of reaction were determined by plotting the natural logarithm of the ratio (C/C_o) against time. The equation

$$ln(C/Co) = -kp.t \tag{4.2}$$

represents the relationship, where "t" represents time in minutes, (C/C_o) denotes the "ratio of concentration" at any time to the initial concentration (mg/L), and "kp" signifies the "photocatalytic rate constant" (min^{-1}).
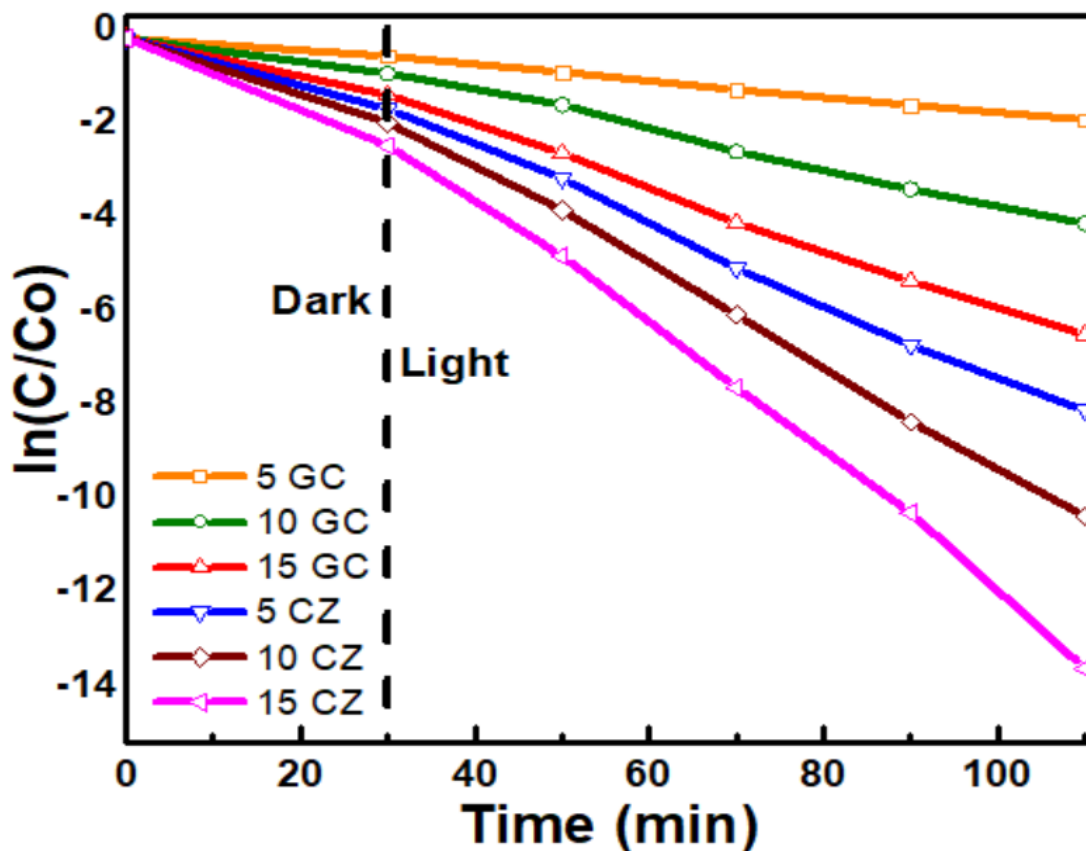
Figure 4.10: Kinetics of all hybrids.

The figure clearly demonstrates that the kinetics of tetracycline decomposition adhere to a first-order rate model for all photocatalysts, with R^2 values exceeding 0.90 for each. Approximately 40% of degradation occurs within the first half-hour. In the presence of light, degradation proceeds rapidly due to the photoactive nature of nanohybrids. All things considered, of all the synthesized photocatalysts, 15CZ exhibited the highest tetracycline removal efficiency, removing a maximum of 96%. Since R^2 values are greater

than 0.90, it indicates that all the synthesized photocatalysts conform to a first order fit and exhibit strong activity in the photocatalytic process. While investigating the reaction kinetics for photo catalysis pseudo first order was fitted. All of catalyst show R^2 values greater than 0.9 which is consistent with the reaction order fit. Rate constant for the 15CZ is higher as compared to all due to presence of heterojunction and high number of electron and hole pair generation. 10CZ shows the second highest removal kinetics because of formation of heterojunction. CZ shows the removal kinetics due to presence of visible light active CdS onto ZIF-67.

Table 4.2: Photocatalytic activity of all synthesized hybrids

Material	"Photocatalyst/ Adsorbent"	R^2	"Removal Efficiency ((Co-C)/Co) *100"	"Rate Constant min^{-1} (photocatalysis) l/min (Adsorption) "	"Order of reaction (n) "
5 mg g-C_3N_4@CdS	Good	0.99557	82.429	-0.0162	n = 1
10 mg g-C_3N_4@CdS	Better	0.97223	89.04183	-0.02108	n = 1
15 mg g-C_3N_4@CdS	Better	0.99225	90.69952	-0.02238	n = 1
5 mg CdS@ZIF-67	Good	0.97414	80.08291	-0.01546	n = 1

10 mg CdS@ZIF-67	Better	0.94148	89.49845	-0.02051	n = 1
15 mg CdS@ZIF-67	Best	0.92258	96.12614	-0.02788	n = 1

The rate constant, measured in min^{-1} through linear fit, reveals an interesting trend. The rate constant having values -0.0162 for 5GC, -0.02108 for 10GC, and -0.02238 for 15GC. For the 5CZ, 10CZ, and 15CZ nanohybrids, the "rate constant values" are -0.01546, -0.02051, and -0.02788, respectively. These rate constant values increase as the concentration of the hybrid materials increases from 5 mg to 15 mg, indicating a substantial dependence on the adsorption of tetracycline on photocatalyst surface.

4.3.2   Possible Mechanism

Possible mechanism of adsorption can be due to fact that moreover there are different ionic forms of tetracycline molecule depending on PH of the solvent. For example, in PH range of 0-5 it exists as positive ion form 5-8 it exists as Zwitter ion and up to PH 11 it is in negative ion. Since stock solution of tetracycline was made in the deionized water having PH value of 7. Thus, tetracycline in this condition will exist as zwitter ion. Electropositive species in these hybrids will also develop interaction with negative poles of zwitter ion.

Hence electrostatic interaction and π-π interaction contribute to enhance adsorption of tetracycline onto the surface of hybrid. Due to enhancement in mesoporosity of g-C_3N_4, CdS adsorption also enhances. This can arise because of increment in active sites of π-π bonding among nitrogen on g-C_3N_4 coupled with CdS rods. Because as in the structure of g-C_3N_4 it is composed of heptazine units which is verified by DFT calculation. And in each heptazine unit beside N2 there is gap formed due to contribution of these N2s. This gap serves as propose of adsorption site because of mesoporosity. Increase in adsorption while

increasing the graphitic carbon nitride content in GC hybrids signifies that mesoprosity enhancement in GC leads to increase in adsorption. Flattening of curves of tetracycline removal by adsorption with time is due to attainment of equilibrium concentration by as synthesized GC and CZ series.

The reaction mechanism of photocatalysis has been discussed. In the first phase after attack of electron hole pair hydroxylation of tetracycline molecule takes place. After that tetracycline molecules become dehydrated. At the end demethylation of molecules occurs. Finally, ring opening happens of tetracycline. Ring opening product further oxidized to the CO_2 and H_2O. This process implies that no harmful products are produced, and the process is beneficial to the environment. Trend was such that increase in g-C_3N_4 and CdS content in the GC and CZ series respectively lead to increase in percentage removal because of increase in all dominant factors such as surface area, mesoporisity and large numbers of hole and electron pair generation.

CHAPTER 5: CONCLUSIONS AND FUTURE RECOMMENDATIONS

5.1 Conclusions:

We effectively synthesized the high-efficiency advanced nanohybrid material g-C_3N_4@CdS and CdS@ZIF-67 in this work. Zeolite Imidazole Frameworks (ZIFs) were synthesized in the present research by integrating economical metal salts of zinc and cobalt with chemically designed imidazole organic bridging units of 2-methylimidazole. Once tested under specific conditions, this composite exhibited photocatalysis activity. All the catalysts have been synthesized using a hydrothermal and in-situ process. The nanohybrids were defined by SEM and XRD, confirming that nanohybrids were successfully formed. The band gap of nanohybrid material has been analyzed using UV-VIS. The photocatalytic performance of g- C_3N_4@CdS and CdS@ZIF-67 were examined using varied concentrations of C_3N_4 and CdS respectively. The photocatalyst experiment was completed successfully at PH=7. By using 100 mg of CdS@ZIF-67 hybrid, 96% of tetracycline has been successfully degraded in 110 minutes. The OH radical played an integral part in photocatalysis. Adsorption was caused by electrostatic interactions and the contribution of π-π bonds. Adsorbent mesoporosity and microporosity also influenced the adsorption efficiency trends. It is reasonable to assume that the catalyst worked well for treating wastewater and hospital sludge with high TC concentrations.

Environmental safety is also demonstrated by the formation of a catalyst and photocatalytic activity for removing tetracycline from water. This could pave the way for new processes to replace existing ones, such as the membrane-facilitated activated sludge process. Other processes, such as biological, can also be significantly replaced by photocatalysis using synthesized hybrids. Because such a catalyst does not produce any intermediate or product that is reactive or toxic to the environment. A more complete mineralization of photocatalysis by these hybrids ensures that tetracycline is perfectly oxidized and reduced to CO_2 and H_2O, resulting in environmental safety.

5.2 Future Recommendation

The primary concern is the development of an efficient reactor model that can successfully integrate the synthesized catalyst to perform pollutant degradation such as TC [116]. Various models have been used in the past, such as an immobilized form of catalyst supported on borosilicate glass. A collector with a specific quantum efficacy is provided in this sort of reactor. A photocatalytic reaction occurred when these discs were rotated at specific revolutions per minute because of the concentration of specific intensity light onto the surface of an immobilized catalyst supported on borosilicate glass. A specific inlet and outlet are provided to handle the feed. The problem with these types of reactors is that the catalyst's recovery is very low.

The three-phase fluidized bed, which can be used for manufacturing the catalyst mentioned above, is another apparent type of catalyst reactor. Such a reactor needs to have a separate compartment constructed of solvent-proof borosilicate glass. Through the bottom pipe beneath the compartments', dissolved oxygen is used to circulate the catalyst suspension as it enters the reactor from the inlet feed. Three phases exist as a result of dissolved oxygen acting as a fluidization catalyst. As a result, process effectiveness is raised. The light intensity can be altered in accordance with the reactor's residence time, which is determined by the kinetics of the reaction. For the reactor configuration, steady-state calculations can be performed.

It is possible to conduct active species trapping experiments using various agents. For instance, a variety of radicals, including OH, benzoquinone, and IPA, function as masking agents for certain ROS, such as O_2. Using UV-VIS analysis, these can be seen and identified which can confirm that the species is actively involved in the degradation of tetracycline by means of these experiments.

Future research into CdS based materials should be geared towards enhancing their potential for industrial applications. This can be accomplished by exploring treatment systems capable of removing multiple pollutants instead of focusing solely on individual target compounds. To achieve this, it is advisable to conduct tests using real wastewater samples and investigate the effects influent salt content and PH on the pollutant decomposition procedure. This transition from laboratory-scale experiments to pilot-scale

setups would be a significant advancement. Furthermore, the development of easier and more environmentally friendly methods of synthesis CdS composites and integrating these materials with substrates offers promising avenues for technological advancement.

REFERENCES

[1] Z. S. Yuan, J. X. Zou, X. L. Zhao, J. Y. Shi, C. S. Guo, and M. Yan, "Cadmium sulfide cage photocatalysis coupled electroactive biofilm for synergistic promotion of tetracycline degradation and electricity production," *Journal of Materials Science & Technology,* 2023.

[2] G. A. Khan, B. Berglund, K. M. Khan, P.-E. Lindgren, and J. J. P. o. Fick, "Occurrence and abundance of antibiotics and resistance genes in rivers, canal and near drug formulation facilities–a study in Pakistan," vol. 8, no. 6, p. e62712, 2013.

[3] G. Gopal, S. A. Alex, N. Chandrasekaran, and A. Mukherjee, "A review on tetracycline removal from aqueous systems by advanced treatment techniques," *RSC advances,* vol. 10, no. 45, pp. 27081-27095, 2020.

[4] Y. Gao *et al.*, "Adsorption and removal of tetracycline antibiotics from aqueous solution by graphene oxide," *Journal of colloid and interface science,* vol. 368, no. 1, pp. 540-546, 2012.

[5] L. Zhang, X. Song, X. Liu, L. Yang, F. Pan, and J. Lv, "Studies on the removal of tetracycline by multi-walled carbon nanotubes," *Chemical engineering journal,* vol. 178, pp. 26-33, 2011.

[6] H. Liu, Y. Yang, J. Kang, M. Fan, and J. Qu, "Removal of tetracycline from water by Fe-Mn binary oxide," *Journal of environmental sciences,* vol. 24, no. 2, pp. 242-247, 2012.

[7] U. Abdullah, M. Ali, and E. J. M. C. Pervaiz, "An inclusive review on recent advancements of cadmium sulfide nanostructures and its hybrids for photocatalytic and electrocatalytic applications," vol. 508, p. 111575, 2021.

[8] C. V. Gómez-Pacheco, M. Sánchez-Polo, J. Rivera-Utrilla, and J. López-Peñalver, "Tetracycline removal from waters by integrated technologies based on ozonation and biodegradation," *Chemical engineering journal,* vol. 178, pp. 115-121, 2011.

[9] Y. Dai *et al.*, "A review on pollution situation and treatment methods of tetracycline in groundwater," *Separation science and technology,* vol. 55, no. 5, pp. 1005-1021, 2020.

[10] S. Sharma, V. Dutta, P. Raizada, A. Hosseini-Bandegharaei, P. Singh, and V.-H. Nguyen, "Tailoring cadmium sulfide-based photocatalytic nanomaterials for water decontamination: a review," *Environmental Chemistry Letters,* vol. 19, pp. 271-306, 2021.

[11]   H. Sereshti *et al.*, "Sulfide-Doped Magnetic Carbon Nanotubes Developed as Adsorbent for Uptake of Tetracycline and Cefixime from Wastewater," vol. 12, no. 20, p. 3576, 2022.

[12]   H. Xiong, S. Dong, J. Zhang, D. Zhou, and B. E. Rittmann, "Roles of an easily biodegradable co-substrate in enhancing tetracycline treatment in an intimately coupled photocatalytic-biological reactor," *Water research,* vol. 136, pp. 75-83, 2018.

[13]   L. Shao, Z. Ren, G. Zhang, and L. Chen, "Facile synthesis, characterization of a MnFe2O4/activated carbon magnetic composite and its effectiveness in tetracycline removal," *Materials Chemistry and Physics,* vol. 135, no. 1, pp. 16-24, 2012.

[14]   A. Balakrishnan, M. Chinthala, R. K. Polagani, and D.-V. N. Vo, "Removal of tetracycline from wastewater using g-C3N4 based photocatalysts: A review," *Environmental Research,* p. 114660, 2022.

[15]   D. S. Pattanayak, D. Pal, J. Mishra, C. Thakur, and K. L. Wasewar, "Doped graphitic carbon nitride (g-C3N4) catalysts for efficient photodegradation of tetracycline antibiotics in aquatic environments," *Environmental Science and Pollution Research,* vol. 30, no. 10, pp. 24919-24926, 2023.

[16]   H. Fang, Y. Han, X. Feng, W. Ji, and C.-T. Au, "S-scheme heterojunction g-C3N4/Ag/AgNCO for efficient tetracycline removal in a photo-assisted peroxymonosulfate system," *Separation and Purification Technology,* vol. 296, p. 121210, 2022.

[17]   Y. Yang, Z. Bian, L. Zhang, and H. Wang, "Bi@ BiOx (OH) y modified oxidized g-C3N4 photocatalytic removal of tetracycline hydrochloride with highly effective oxygen activation," *Journal of Hazardous Materials,* vol. 427, p. 127866, 2022.

[18]   X. Zhang *et al.*, "High-efficiency removal of tetracycline by carbon-bridge-doped g-C3N4/Fe3O4 magnetic heterogeneous catalyst through photo-Fenton process," *Journal of Hazardous Materials,* vol. 418, p. 126333, 2021.

[19]   L. Kong, J. Wang, F. Ma, M. Sun, and J. J. A. M. T. Quan, "Graphitic carbon nitride nanostructures: Catalysis," vol. 16, pp. 388-424, 2019.

[20]   H. B. Truong, S. Bae, J. Cho, and J. Hur, "Advances in application of g–C3N4–based materials for treatment of polluted water and wastewater via activation of oxidants and photoelectrocatalysis: A comprehensive review," *Chemosphere,* vol. 286, p. 131737, 2022/01/01/ 2022.

[21]   G. Dong, Y. Zhang, Q. Pan, J. J. J. o. P. Qiu, and P. C. P. Reviews, "A fantastic graphitic carbon nitride (g-C3N4) material: electronic structure, photocatalytic and photoelectronic properties," vol. 20, pp. 33-50, 2014.

[22] T. An *et al.*, "Photoelectrochemical conversion from graphitic C3N4 quantum dot decorated semiconductor nanowires," vol. 8, no. 20, pp. 12772-12779, 2016.

[23] C. Hu, Y.-C. Chu, M.-S. Wang, X.-H. J. J. o. P. Wu, and P. A. Chemistry, "Rapid synthesis of g-C3N4 spheres using microwave-assisted solvothermal method for enhanced photocatalytic activity," vol. 348, pp. 8-17, 2017.

[24] Y. Zheng, Z. Zhang, C. J. J. o. P. Li, and P. A. Chemistry, "A comparison of graphitic carbon nitrides synthesized from different precursors through pyrolysis," vol. 332, pp. 32-44, 2017.

[25] H. Dong, X. Guo, C. Yang, and Z. J. A. C. B. E. Ouyang, "Synthesis of g-C3N4 by different precursors under burning explosion effect and its photocatalytic degradation for tylosin," vol. 230, pp. 65-76, 2018.

[26] X. Tan, L. Kou, H. A. Tahini, and S. C. J. S. r. Smith, "Conductive graphitic carbon nitride as an ideal material for electrocatalytically switchable CO2 capture," vol. 5, no. 1, p. 17636, 2015.

[27] H. Li, Z. Zhang, Y. Liu, W. Cen, and X. J. N. Luo, "Functional group effects on the HOMO–LUMO gap of g-C3N4," vol. 8, no. 8, p. 589, 2018.

[28] F. Wei *et al.*, "Oxygen self-doped gC 3 N 4 with tunable electronic band structure for unprecedentedly enhanced photocatalytic performance," vol. 10, no. 9, pp. 4515-4522, 2018.

[29] H. Dong, A. R. Oganov, Q. Zhu, and G.-R. J. S. r. Qian, "The phase diagram and hardness of carbon nitrides," vol. 5, no. 1, pp. 1-5, 2015.

[30] Y. Yang *et al.*, "Recent advances in application of graphitic carbon nitride-based catalysts for degrading organic contaminants in water through advanced oxidation processes beyond photocatalysis: A critical review," vol. 184, p. 116200, 2020.

[31] L. Zhang *et al.*, "Recent Advances in Application of Graphitic Carbon Nitride-Based Catalysts for Photocatalytic Nitrogen Fixation," vol. 18, no. 28, p. 2202252, 2022.

[32] R. Hu, X. Wang, S. Dai, D. Shao, T. Hayat, and A. J. C. E. J. Alsaedi, "Application of graphitic carbon nitride for the removal of Pb (II) and aniline from aqueous solutions," vol. 260, pp. 469-477, 2015.

[33] F. Liang and Y. J. A. C. B. E. Zhu, "Enhancement of mineralization ability for phenol via synergetic effect of photoelectrocatalysis of g-C3N4 film," vol. 180, pp. 324-329, 2016.

[34] X. L. Wang and H. G. J. A. C. B. E. Yang, "Facile fabrication of high-yield graphitic carbon nitride with a large surface area using bifunctional urea for enhanced photocatalytic performance," vol. 205, pp. 624-630, 2017.

[35] S. Sun and S. J. N. Liang, "Recent advances in functional mesoporous graphitic carbon nitride (mpg-C 3 N 4) polymers," vol. 9, no. 30, pp. 10544-10578, 2017.

[36] W.-J. Ong, L.-L. Tan, Y. H. Ng, S.-T. Yong, and S.-P. J. C. r. Chai, "Graphitic carbon nitride (g-C3N4)-based photocatalysts for artificial photosynthesis and environmental remediation: are we a step closer to achieving sustainability?," vol. 116, no. 12, pp. 7159-7329, 2016.

[37] K. An *et al.*, "Biomimetic synthesis of 2D/2D mixed graphitic carbon nitride/carbonized polydopamine nanosheets with excellent photocatalytic performance," vol. 256, p. 123621, 2020.

[38] Y. Zang, L. Li, X. Li, R. Lin, and G. J. C. E. J. Li, "Synergistic collaboration of g-C3N4/SnO2 composites for enhanced visible-light photocatalytic activity," vol. 246, pp. 277-286, 2014.

[39] T. Ma, J. Bai, and C. J. V. Li, "Facile synthesis of g-C3N4 wrapping on one-dimensional carbon fiber as a composite photocatalyst to degrade organic pollutants," vol. 145, pp. 47-54, 2017.

[40] Y. Hong *et al.*, "Efficient and stable Nb2O5 modified g-C3N4 photocatalyst for removal of antibiotic pollutant," vol. 299, pp. 74-84, 2016.

[41] X. Dong and F. J. J. o. M. C. A. Cheng, "Recent development in exfoliated two-dimensional gC 3 N 4 nanosheets for photocatalytic applications," vol. 3, no. 47, pp. 23642-23652, 2015.

[42] G. Mamba and A. J. A. C. B. E. Mishra, "Graphitic carbon nitride (g-C3N4) nanocomposites: a new and exciting generation of visible light driven photocatalysts for environmental pollution remediation," vol. 198, pp. 347-377, 2016.

[43] T. S. Natarajan, K. R. Thampi, and R. J. J. A. C. B. E. Tayade, "Visible light driven redox-mediator-free dual semiconductor photocatalytic systems for pollutant degradation and the ambiguity in applying Z-scheme concept," vol. 227, pp. 296-311, 2018.

[44] J.-Y. Hu, K. Tian, and H. J. C. Jiang, "Improvement of phenol photodegradation efficiency by a combined g-C3N4/Fe (III)/persulfate system," vol. 148, pp. 34-40, 2016.

[45] X. Wang, G. Wang, S. Chen, X. Fan, X. Quan, and H. J. J. o. M. S. Yu, "Integration of membrane filtration and photoelectrocatalysis on g-C3N4/CNTs/Al2O3 membrane with visible-light response for enhanced water treatment," vol. 541, pp. 153-161, 2017.

[46]   S. Sharma, V. Dutta, P. Raizada, A. Hosseini-Bandegharaei, P. Singh, and V.-H. J. E. C. L. Nguyen, "Tailoring cadmium sulfide-based photocatalytic nanomaterials for water decontamination: a review," vol. 19, pp. 271-306, 2021.

[47]   H. Xiong, S. Dong, J. Zhang, D. Zhou, and B. E. J. W. r. Rittmann, "Roles of an easily biodegradable co-substrate in enhancing tetracycline treatment in an intimately coupled photocatalytic-biological reactor," vol. 136, pp. 75-83, 2018.

[48]   L. Shao, Z. Ren, G. Zhang, L. J. M. C. Chen, and Physics, "Facile synthesis, characterization of a MnFe2O4/activated carbon magnetic composite and its effectiveness in tetracycline removal," vol. 135, no. 1, pp. 16-24, 2012.

[49]   D. W. Lewis et al., "Zeolitic imidazole frameworks: structural and energetics trends compared with their zeolite analogues," vol. 11, no. 11, pp. 2272-2276, 2009.

[50]   B. Liu and B. J. T. J. o. P. C. C. Smit, "Molecular simulation studies of separation of CO2/N2, CO2/CH4, and CH4/N2 by ZIFs," vol. 114, no. 18, pp. 8515-8522, 2010.

[51]   R. Liang, F. Jing, L. Shen, N. Qin, and L. J. J. o. h. m. Wu, "MIL-53 (Fe) as a highly efficient bifunctional photocatalyst for the simultaneous reduction of Cr (VI) and oxidation of dyes," vol. 287, pp. 364-372, 2015.

[52]   Q. Liu et al., "ZIF-8/Zn 2 GeO 4 nanorods with an enhanced CO 2 adsorption property in an aqueous medium for photocatalytic synthesis of liquid fuel," vol. 1, no. 38, pp. 11563-11569, 2013.

[53]   G. Zhang, G. Kim, W. J. E. Choi, and E. Science, "Visible light driven photocatalysis mediated via ligand-to-metal charge transfer (LMCT): an alternative approach to solar activation of titania," vol. 7, no. 3, pp. 954-966, 2014.

[54]   K.-Y. A. Lin and H.-A. J. C. Chang, "Ultra-high adsorption capacity of zeolitic imidazole framework-67 (ZIF-67) for removal of malachite green from water," vol. 139, pp. 624-631, 2015.

[55]   K. Zhou, B. Mousavi, Z. Luo, S. Phatanasri, S. Chaemchuen, and F. J. J. o. M. C. A. Verpoort, "Characterization and properties of Zn/Co zeolitic imidazolate frameworks vs. ZIF-8 and ZIF-67," vol. 5, no. 3, pp. 952-957, 2017.

[56]   M. A. Fox and M. T. J. C. r. Dulay, "Heterogeneous photocatalysis," vol. 93, no. 1, pp. 341-357, 1993.

[57]   D. F. Ollis, E. Pelizzetti, N. J. E. S. Serpone, and Technology, "Photocatalyzed destruction of water contaminants," vol. 25, no. 9, pp. 1522-1529, 1991.

[58]   J. J. Pignatello, E. Oliveros, A. J. C. r. i. e. s. MacKay, and technology, "Advanced oxidation processes for organic contaminant destruction based on the Fenton reaction and related chemistry," vol. 36, no. 1, pp. 1-84, 2006.

[59] R. Andreozzi, V. Caprio, A. Insola, and R. J. C. t. Marotta, "Advanced oxidation processes (AOP) for water purification and recovery," vol. 53, no. 1, pp. 51-59, 1999.

[60] H. Yao *et al.*, "Hydrothermal synthesis of flower-like Cu2MoS4/g-C3N4 composite and its adsorption performances for Rhodamine B," vol. 223, pp. 648-658, 2019.

[61] Y. Huang, H. Zheng, H. Li, Z. Zhang, Q. Gou, and Y. J. C. E. J. Liu, "Highly effective and selective adsorption of thorium (IV) from aqueous solution using mesoporous graphite carbon nitride prepared by sol–gel template method," vol. 410, p. 128321, 2021.

[62] H. Fattahimoghaddam, T. Mahvelati-Shamsabadi, and B.-K. J. J. o. H. M. Lee, "Efficient photodegradation of rhodamine B and tetracycline over robust and green g-C3N4 nanostructures: supramolecular design," vol. 403, p. 123703, 2021.

[63] M. Wang *et al.*, "Synthesis of hollow lantern-like Eu(III)-doped g-C3N4 with enhanced visible light photocatalytic perfomance for organic degradation," *Journal of Hazardous Materials,* vol. 349, pp. 224-233, 2018/05/05/ 2018.

[64] T. Wu *et al.*, "Tube wall delamination engineering induces photogenerated carrier separation to achieve photocatalytic performance improvement of tubular g-C3N4," *Journal of Hazardous Materials,* vol. 424, p. 127177, 2022/02/15/ 2022.

[65] C. Hu, Z.-T. Liu, P.-C. Yang, Y.-X. Ding, K.-Y. A. Lin, and B.-S. J. J. o. t. T. I. o. C. E. Nguyen, "Self-assembly L-cysteine based 2D g-C3N4 nanoflakes for light-dependent degradation of rhodamine B and tetracycline through photocatalysis," vol. 123, pp. 219-227, 2021.

[66] T. Bhowmik, M. K. Kundu, and S. Barman, "Ultra small gold nanoparticles–graphitic carbon nitride composite: an efficient catalyst for ultrafast reduction of 4-nitrophenol and removal of organic dyes from water," *RSC Advances,* vol. 5, no. 48, pp. 38760-38773, 2015.

[67] K. Li *et al.*, "Fabrication of platinum-deposited carbon nitride nanotubes by a one-step solvothermal treatment strategy and their efficient visible-light photocatalytic activity," *Applied Catalysis B: Environmental,* vol. 165, pp. 428-437, 2015/04/01/ 2015.

[68] Q. Wang *et al.*, "Efficient Organic Dyes Photodegradation Catalyzed by Nickel-Species Loaded Graphitic Carbon Nitride," *Journal of Inorganic and Organometallic Polymers and Materials,* vol. 27, no. 5, pp. 1177-1189, 2017/09/01 2017.

[69] Y. Fu, T. Huang, L. Zhang, J. Zhu, and X. Wang, "Ag/g-C3N4 catalyst with superior catalytic performance for the degradation of dyes: a borohydride-

generated superoxide radical approach," *Nanoscale,* vol. 7, no. 32, pp. 13723-33, Aug 28 2015.

[70] K. Tian, W.-J. Liu, and H. Jiang, "Comparative Investigation on Photoreactivity and Mechanism of Biogenic and Chemosythetic Ag/C3N4 Composites under Visible Light Irradiation," *ACS Sustainable Chemistry & Engineering,* vol. 3, no. 2, pp. 269-276, 2015/02/02 2015.

[71] Z. Chen *et al.*, "Synthesis and fabrication of g-C3N4-based materials and their application in elimination of pollutants," vol. 731, p. 139054, 2020.

[72] J.-Y. Zhang, J.-Y. Mei, S.-S. Yi, and X.-X. J. A. S. S. Guan, "Constructing of Z-scheme 3D g-C3N4-ZnO@ graphene aerogel heterojunctions for high-efficient adsorption and photodegradation of organic pollutants," vol. 492, pp. 808-817, 2019.

[73] J. Rashid, F. Saleemi, B. Akram, L. Wang, N. Hussain, and M. J. N. Xu, "Facile synthesis of g-C3N4/MoO3 nanohybrid for efficient removal of aqueous diclofenac sodium," vol. 11, no. 6, p. 1564, 2021.

[74] M. Wang *et al.*, "Synthesis of hollow lantern-like Eu (III)-doped g-C3N4 with enhanced visible light photocatalytic perfomance for organic degradation," vol. 349, pp. 224-233, 2018.

[75] C. H. Hak *et al.*, "M/gC 3 N 4 (M= Ag, Au, and Pd) composite: synthesis via sunlight photodeposition and application towards the degradation of bisphenol A," vol. 25, pp. 25401-25412, 2018.

[76] K. Li, J. Chen, Y. Ao, P. J. S. Wang, and P. Technology, "Preparation of a ternary g-C3N4-CdS/Bi4O5I2 composite photocatalysts with two charge transfer pathways for efficient degradation of acetaminophen under visible light irradiation," vol. 259, p. 118177, 2021.

[77] D. Li *et al.*, "Synthesis of a carbon dots modified g-C3N4/SnO2 Z-scheme photocatalyst with superior photocatalytic activity for PPCPs degradation under visible light irradiation," vol. 401, p. 123257, 2021.

[78] J. Li, X. Yu, Y. Zhu, X. Fu, Y. J. J. o. A. Zhang, and Compounds, "3D-2D-3D BiOI/porous g-C3N4/graphene hydrogel composite photocatalyst with synergy of adsorption-photocatalysis in static and flow systems," vol. 850, p. 156778, 2021.

[79] M. Clara, B. Strenn, O. Gans, E. Martinez, N. Kreuzinger, and H. J. W. r. Kroiss, "Removal of selected pharmaceuticals, fragrances and endocrine disrupting compounds in a membrane bioreactor and conventional wastewater treatment plants," vol. 39, no. 19, pp. 4797-4807, 2005.

[80] P. Le-Clech, V. Chen, and T. A. J. J. o. m. s. Fane, "Fouling in membrane bioreactors used in wastewater treatment," vol. 284, no. 1-2, pp. 17-53, 2006.

[81]   T. Stephenson, K. Brindle, S. Judd, and B. Jefferson, *Membrane bioreactors for wastewater treatment*. IWA publishing, 2000.

[82]   T. W. Lambert, C. F. Holmes, and S. E. J. W. R. Hrudey, "Adsorption of microcystin-LR by activated carbon and removal in full scale water treatment," vol. 30, no. 6, pp. 1411-1422, 1996.

[83]   A. Bhatnagar, W. Hogland, M. Marques, and M. J. C. E. J. Sillanpää, "An overview of the modification methods of activated carbon for its water treatment applications," vol. 219, pp. 499-511, 2013.

[84]   J. Reungoat, B. Escher, M. Macova, F. Argaud, W. Gernjak, and J. J. W. r. Keller, "Ozonation and biological activated carbon filtration of wastewater treatment plant effluents," vol. 46, no. 3, pp. 863-872, 2012.

[85]   K.-C. Chen, S.-C. Lee, S.-C. Chin, J.-Y. J. E. Houng, and M. Technology, "Simultaneous carbon-nitrogen removal in wastewater using phosphorylated PVA-immobilized microorganisms," vol. 23, no. 5, pp. 311-320, 1998.

[86]   T. E. Agustina, H. M. Ang, V. K. J. J. o. P. Vareek, and P. C. P. Reviews, "A review of synergistic effect of photocatalysis and ozonation on wastewater treatment," vol. 6, no. 4, pp. 264-273, 2005.

[87]   T. Kamiya, J. J. W. S. Hirotsuji, and Technology, "New combined system of biological process and intermittent ozonation for advanced wastewater treatment," vol. 38, no. 8-9, pp. 145-153, 1998.

[88]   P. R. Gogate and A. B. J. A. i. E. R. Pandit, "A review of imperative technologies for wastewater treatment I: oxidation technologies at ambient conditions," vol. 8, no. 3-4, pp. 501-551, 2004.

[89]   H. M. Jang and E. Kan, "Engineered biochar from agricultural waste for removal of tetracycline in water," *Bioresour Technol,* vol. 284, pp. 437-447, Jul 2019.

[90]   H. M. Jang, S. Yoo, Y.-K. Choi, S. Park, and E. Kan, "Adsorption isotherm, kinetic modeling and mechanism of tetracycline on Pinus taeda-derived activated biochar," *Bioresource Technology,* vol. 259, pp. 24-31, 2018.

[91]   S. Álvarez-Torrellas, A. Rodríguez, G. Ovejero, and J. García, "Comparative adsorption performance of ibuprofen and tetracycline from aqueous solution by carbonaceous materials," *Chemical Engineering Journal,* vol. 283, pp. 936-947, 2016.

[92]   J. Hoslett, H. Ghazal, E. Katsou, and H. Jouhara, "The removal of tetracycline from water using biochar produced from agricultural discarded material," *Sci Total Environ,* vol. 751, p. 141755, Jan 10 2021.

[93]   D. Zhang, J. Yin, J. Zhao, H. Zhu, and C. Wang, "Adsorption and removal of tetracycline from water by petroleum coke-derived highly porous activated carbon," *Journal of Environmental Chemical Engineering,* vol. 3, no. 3, pp. 1504-1512, 2015.

[94]   S. Panneri, P. Ganguly, B. N. Nair, A. A. P. Mohamed, K. G. K. Warrier, and U. N. S. Hareesh, "Role of precursors on the photophysical properties of carbon nitride and its application for antibiotic degradation," *Environmental Science and Pollution Research,* vol. 24, pp. 8609-8618, 2017.

[95]   H. Dong, X. Guo, C. Yang, and Z. Ouyang, "Synthesis of g-C3N4 by different precursors under burning explosion effect and its photocatalytic degradation for tylosin," *Applied Catalysis B: Environmental,* vol. 230, pp. 65-76, 2018.

[96]   M. Sturini *et al.*, "gC 3 N 4-promoted degradation of ofloxacin antibiotic in natural waters under simulated sunlight," vol. 24, pp. 4153-4161, 2017.

[97]   D. B. Hernández-Uresti, A. Vázquez, D. Sanchez-Martinez, and S. Obregón, "Performance of the polymeric g-C3N4 photocatalyst through the degradation of pharmaceutical pollutants under UV–vis irradiation," *Journal of Photochemistry and Photobiology A: Chemistry,* vol. 324, pp. 47-52, 2016.

[98]   F. Wang *et al.*, "Photocatalytic degradation of fluoroquinolone antibiotics using ordered mesoporous g-C3N4 under simulated sunlight irradiation: kinetics, mechanism, and antibacterial activity elimination," *Applied Catalysis B: Environmental,* vol. 227, pp. 114-122, 2018.

[99]   W. Wang, J. Fang, and H. Chen, "Nano-confined g-C3N4 in mesoporous SiO2 with improved quantum size effect and tunable structure for photocatalytic tetracycline antibiotic degradation," *Journal of Alloys and Compounds,* vol. 819, p. 153064, 2020.

[100]   X. Wang, Q. Liu, Q. Yang, Z. Zhang, and X. Fang, "Three-dimensional g-C3N4 aggregates of hollow bubbles with high photocatalytic degradation of tetracycline," *Carbon,* vol. 136, pp. 103-112, 2018.

[101]   C. Zhou *et al.*, "Visible-light-driven photocatalytic degradation of sulfamethazine by surface engineering of carbon nitride: Properties, degradation pathway and mechanisms," *Journal of hazardous materials,* vol. 380, p. 120815, 2019.

[102]   S. N. Frank and A. J. J. T. j. o. p. c. Bard, "Heterogeneous photocatalytic oxidation of cyanide and sulfite in aqueous solutions at semiconductor powders," vol. 81, no. 15, pp. 1484-1488, 1977.

[103]   L.-L. Feng *et al.*, "Nanoporous sulfur-doped graphitic carbon nitride microrods: A durable catalyst for visible-light-driven H2 evolution," vol. 39, no. 28, pp. 15373-15379, 2014.

[104] P. Madhusudan, J. Zhang, B. Cheng, and J. J. P. C. C. P. Yu, "Fabrication of CdMoO 4@ CdS core–shell hollow superstructures as high performance visible-light driven photocatalysts," vol. 17, no. 23, pp. 15339-15347, 2015.

[105] H. Park, Y. Park, W. Kim, W. J. J. o. P. Choi, and P. C. P. Reviews, "Surface modification of TiO2 photocatalyst for environmental applications," vol. 15, pp. 1-20, 2013.

[106] H. Yao *et al.*, "Hydrothermal synthesis of flower-like Cu2MoS4/g-C3N4 composite and its adsorption performances for Rhodamine B," *Materials Chemistry and Physics,* vol. 223, pp. 648-658, 2019/02/01/ 2019.

[107] Y. Zou *et al.*, "β-Cyclodextrin modified graphitic carbon nitride for the removal of pollutants from aqueous solution: experimental and theoretical calculation study," *Journal of Materials Chemistry A,* 10.1039/C6TA05958A vol. 4, no. 37, pp. 14170-14179, 2016.

[108] M. R. Rajeshwari, S. Kokilavani, and S. S. J. C. Khan, "Recent developments in architecturing the g-C3N4 based nanostructured photocatalysts: Synthesis, modifications and applications in water treatment," vol. 291, p. 132735, 2022.

[109] X. Wang *et al.*, "A metal-free polymeric photocatalyst for hydrogen production from water under visible light," vol. 8, no. 1, pp. 76-80, 2009.

[110] X. Wang, S. Blechert, and M. J. A. C. Antonietti, "Polymeric graphitic carbon nitride for heterogeneous photocatalysis," vol. 2, no. 8, pp. 1596-1606, 2012.

[111] S. Zhang *et al.*, "In situ synthesis of water-soluble magnetic graphitic carbon nitride photocatalyst and its synergistic catalytic performance," vol. 5, no. 23, pp. 12735-12743, 2013.

[112] Y. Chen *et al.*, "Supramolecular electrostatic self-assembly of mesoporous thin-walled graphitic carbon nitride microtubes for highly efficient visible-light photocatalytic activities," vol. 49, pp. 214-223, 2020.

[113] G. Mamba and A. K. Mishra, "Graphitic carbon nitride (g-C3N4) nanocomposites: A new and exciting generation of visible light driven photocatalysts for environmental pollution remediation," *Applied Catalysis B: Environmental,* vol. 198, pp. 347-377, 2016/12/05/ 2016.

[114] T. Ma, J. Bai, and C. Li, "Facile synthesis of g-C3N4 wrapping on one-dimensional carbon fiber as a composite photocatalyst to degrade organic pollutants," *Vacuum,* vol. 145, pp. 47-54, 2017/11/01/ 2017.

[115] J. Li *et al.*, "Synthesis of MoS2/g-C3N4 nanosheets as 2D heterojunction photocatalysts with enhanced visible light activity," *Applied Surface Science,* vol. 364, pp. 694-702, 2016.

[116] T. Sauer, G. C. Neto, H. Jose, R. J. J. o. P. Moreira, and P. A. Chemistry, "Kinetics of photocatalytic degradation of reactive dyes in a TiO2 slurry reactor," vol. 149, no. 1-3, pp. 147-154, 2002.